THE UNIVERSITY OF ALBERTA

FOURIER TRANSFORM INFRARED IN-SITU SPECTROELECTROCHEMISTRY

by

© Timothy Marc Davidson

A THESIS

SUBMITTED TO THE FACULTY OF GRADUATE STUDIES AND RESEARCH IN PARTIAL FULFILMENT OF THE REQUIREMENTS FOR THE DEGREE OF MASTER OF SCIENCE

DEPARTMENT OF CHEMISTRY

EDMONTON, ALBERTA

SPRING 1983

THE UNIVERSITY OF ALBERTA

RELEASE FORM

NAME OF AUTHOR Timothy Marc Davidson

TITLE OF THESIS Fourier Transform Infrared In-situ Spectroelectrochemistry

DEGREE FOR WHICH THESIS WAS PREPARED M.Sc.

YEAR THIS DEGREE GRANTED 1983

Permission is hereby granted to THE UNIVERSITY OF ALBERTA LIBRARY to reproduce single copies of this thesis and to lend or sell such copies for private, scholarly or scientific research purposes only.

The author reserves other publication rights, and neither the thesis nor extensive extracts from it may be printed or otherwise reproduced without the author's written permission.

(Signed) Timothy M. Davidson

PERMANENT ADDRESS

263 N. Belle River Avenue
Marine City, Michigan 48039, U.S.A.

DATE Jan 10 1983

THE UNIVERSITY OF ALBERTA

FACULTY OF GRADUATE STUDIES AND RESEARCH

The undersigned certify that they have read, and recommend to the Faculty of Graduate Studies and Research, for acceptance, a thesis entitled:

FOURIER TRANSFORM INFRARED IN-SITU SPECTROELECTROCHEMISTRY

submitted by TIMOTHY MARC DAVIDSON in partial fulfilment of the requirements for the degree of Master of Science.

.....

Supervisor

.....

.....

DATE JAN 10, 1983

To my mother and father

ABSTRACT

In this study, the successful application of Fourier transform infrared spectroscopy to the in-situ investigation of the electrode-electrolyte solution interphase has been accomplished. The new method was used to study the double layer region of a platinum mirror electrode in acetonitrile solutions. With this new technique, it is possible to observe changes in the vibrational structure of the interfacial region between two potential states. This is accomplished by subtracting the reflection — absorbance spectra obtained at each of the potentials. The technique is a single reflection experiment. Radiation is passed through a thin optically transparent window, a very thin layer of solution, is reflected from the electrode of interest back through the solution, and out of the cell to a suitable detector.

The new technique was also used to obtain the infrared spectra of organic molecular ion radicals generated at an oxidizing or reducing electrode. Thus, for the first time, it is possible to study in-situ the changes that occur in the vibrational structure of a molecule as it undergoes electron transfer reactions.

The work demonstrates the speed and versatility of what appears to be a valuable new tool in the study of surface processes.

ACKNOWLEDGEMENTS

I would like to thank Dr. B. Stanley Pons for the opportunity to do research on such an interesting project. His help throughout the project is sincerely appreciated.

I wish also to thank Dr. John E. Bertie for his helpful discussions on vibrational theory and his guidance on the interferometer operation.

Finally I would like to thank Dr. Alan Bewick for his many helpful ideas. Tribute must also be paid to spectral services, machine shop, electronic shop and glass shop for their prompt services.

TABLE OF CONTENTS

	page
Abstract	v
Acknowledgements	vi
List of Tables	ix
List of Figures	xii
Chapter 1 Introduction	1
1.1 Object	1
1.2 Background	2
1.3 Solution free Measurements	6
1.4 Surface Studies	12
Chapter 2 Experimental	15
2.1 Preparations	15
2.1.1 Purification of Acetonitrile	15
2.1.2 Preparation of Tetra-n-butylammonium-Tetrafluoroborate	17
2.1.3 Purification of Commercial Chemicals	18
2.2 Optical Cell and Electrodes	18
2.3 Instrumentation	26
2.3.1 Spectrometer	26
2.4 Apparatus	39
2.5 Data Collection	42
Chapter 3 Double Layer Structure	54
3.1 Results	54
3.2 Discussion	64
3.3 Conclusion	82

page

Chapter 4 Solution Free Measurements..... 83

4.1 Results..... 83

4.2 Discussion..... 101

4.3 Conclusion..... 106

References..... 107

Appendix..... 114

LIST OF TABLES

Table — Page

1. References for Spectroelectrochemical Methods..... 5

2. Band Positions for Difference Spectra of 0.1M Tetrabutylammonium Tetrafluoroborate in Acetonitrile..... 56

3. Band Positions for Difference Spectra of 0.1M Tetrabutylammonium Tetrafluoroborate and 0.1M Water in Acetonitrile..... 59

4. Band Positions for Difference Spectra of 0.1M Lithium Perchlorate in Acetonitrile..... 62

5. Band Positions for Difference Spectra of 0.1M Lithium Perchlorate and 0.1M Water in Acetonitrile..... 65

6. Band Positions for Difference Spectra of 0.1M Lithium Hexafluoroarsenate in Acetonitrile..... 67

Table Page

7. Band Positions for Difference Spectra of 0.1M Lithium Perchlorate in Acetonitrile with 0.006% Water (Gold Electrode)..... 69

8. Band Positions for Infrared Spectrum of Acetonitrile.... 71

9. Some Band Positions for Infrared Spectra of 0.1M Electrolytes in Acetonitrile..... 75

10. Band Positions for Difference Spectrum of 0.01M Benzophenone in Acetonitrile with 0.1M TBAF and Pulsed from -1.75V to -2.5V vs Ag/Ag+ Reference..... 85

11. Some Band Positions for an Infrared Spectrum of Benzophenone in Acetonitrile..... 88

12. Band Positions for Difference Spectrum of 0.005M Anthracene in Acetonitrile with 0.1M TBAF and Pulsed from -1.5V to -2.5V vs Ag/Ag+ Reference..... 90

13. Band Positions for an Infrared Spectrum of Anthracene (KBr Disc.)..... 94

Table | Page

14. Band Positions for Difference Spectrum of 0.005M Tetracyanoethylene in Acetonitrile with 0.1M TBAF and Pulsed from +0.25V to -0.25V vs Ag/Ag+ Reference..... 96

15. Band Positions for an Infrared Spectrum of Tetracyanoethylene in KBr Disc..... 100

16. Comparison of Band Positions for Benzophenone Anion Radical..... 102

17. Comparison of Band Positions for Anthracene Anion Radical..... 104

LIST OF FIGURES

Figure		Page
1.	IR Electrochemical Cell.....	19
2.	The Polishing Mandril for the Mirror Working Electrode.....	21
3.	The Path of the Infrared Beam Through the Cell.....	23
4.	Simplified Diagram of the Nicolet 7199 Spectrometer.....	27
5.	Cosine Wave Interferogram.....	29
6.	Typical Mid-Infrared Interferogram.....	32
7.	Instrument Line shape: the Function Sin x/x.....	34
8.	Apparatus Setup in Spectrometer.....	40
9.	Electrochemical Reflectance Cell Holder.....	41
10.	Counter Circuit.....	43

Figure		Page
11.	Difference Absorption Band Type I.....	47
12.	Difference Absorption Band Type II.....	48
13.	Difference Absorption Band Type III.....	49
14.	Concentration Profile of Electrogenerated Species vs Time.....	52
15.	Difference Spectra of 0.1M Tetrabutylammonium Tetrafluoroborate in Acetonitrile.....	55
16.	Difference Spectra of 0.1M Tetrabutylammonium Tetrafluoroborate and 0.1M Water in Acetonitrile.....	58
17.	Difference spectra of 0.1M Lithium Perchlorate in Acetonitrile.....	61
18.	Difference Spectra of 0.1M Lithium Perchlorate and 0.1M Water in Acetonitrile.....	63
19.	Difference Spectra of 0.1M Lithium Hexafluoroarsenate in Acetonitrile.....	66

Figure Page

20. Difference Spectra of 0.1M Lithium Perchlorate in Acetonitrile with 0.006% Water (Gold Electrode)..... 68

21. Infrared Spectrum of Acetonitrile..... 70

22. Infrared Spectrum of 0.1M Lithium Perchlorate in Acetonitrile (Acetonitrile subtracted from Spectrum)..... 72

23. Infrared Spectrum of 0.1M Lithium Hexafluorarsenate in Acetonitrile (Acetonitrile subtracted from Spectrum)..... 73

24. Infrared Spectrum of 0.1M Tetrabutylammonium Tetrafluoroborate in Acetonitrile (Acetonitrile Subtracted from Spectrum)..... 74

25. Infrared Difference Spectrum of 0.01M Benzophenone in Acetonitrile with 0.1M TBAF and Pulsed from -1.75V to -2.5V vs Ag/Ag+ Reference 84

Figure Page

26. Cyclic Voltammogram of 0.01 M Benzophenone in Acetonitrile with 0.1M TBAF.....86

27. Infrared Spectrum of 0.2M Benzophenone in Acetonitrile (Acetonitrile subtracted from Spectrum)..... 87

28. Infrared Difference Spectrum of 0.005M Anthracene in Acetonitrile with 0.1M TBAF and Pulsed from -1.5V to -2.5V vs Ag/Ag+ Reference..... 89

29. Cyclic Voltammogram of 0.005M Anthracene in Acetonitrile with 0.1M TBAF..... 92

30. Infrared Spectrum of Anthracene (KBr Disc.)..... 93

31. Infrared Difference Spectrum of 0.005M Tetracyanoethylene in Acetonitrile with 0.1M TBAF and Pulsed from +0.25V to -0.25V vs Ag/Ag+ Reference..... 95

32. Figure 31 Expanded..... 97

CHAPTER 1

INTRODUCTION

1.1 Objective

The object of this thesis is to determine and develop a way in which to describe, and understand the structure of the electrode-electrolyte interphase. The structural information of the electrode interphase can give insight into the mechanisms of catalysis directly. Thus, it would be possible to determine how to inhibit or accelerate catalytic processes.

The method used in this thesis is modulated infrared reflection spectroelectrochemistry (1-6, 84-86). The infrared light is passed through solution and reflected from an electrode surface back through solution. The method monitors changes in the interphase optically during an electrochemical experiment without affecting the interphase.

Other techniques used to study the electrode interphase are either not completely understood, or the electrode is removed from solution in order to study it. When an electrode is moved from a solution to a vacuum, there is undoubtedly a change in the interphase. Considering the currently available techniques, modulated infrared reflection spectroelectrochemistry will be shown to be the best way to study the electrode interphase in-situ.

This research was the first time that a Fourier transform infrared spectrometer was used in modulated infrared reflection spectroelectrochemistry (4).

During this research it was also found that the technique of modulated infrared reflection spectroelectrochemistry could be used to obtain infrared spectra of electrochemically generated intermediates (85). This will be discussed later.

1.2 Background

A study of electrochemical processes occurring at the electrode surface by an optical spectroscopic method was first made in 1964 (7). The technique was dubbed spectroelectrochemistry. Since then, it has been adopted by many electrochemists as a means for monitoring different processes occurring at or near the electrode surface. Thus one is able to observe spectrally the effects of adsorption (1-6, 8-14, 16, 37), double layer structure (2-6, 15, 16, 84-86), kinetics of homogeneous reactions in the diffuse layer (17-26, 35), processes of catalysis (15-16), the point of zero charge, and metal deposition (27-28).

Spectroelectrochemical techniques are usually not more sensitive than normal electrochemical methods, but are more specific to individual processes in the interphase. This is due to the fact that, in general, electrochemical methods measure all the processes occurring at the interphase. Thus by normal electrochemical methods the structure of the reaction intermediates can only be determined by assumption after isolating the reaction products. This makes the determination of

reaction mechanisms somewhat more dubious than spectroelectrochemical techniques where direct observation of individual intermediates is possible.

Certain spectroelectrochemical techniques can give information on the vibrational structure of the molecules in their environment at the electrode interphase. Other spectroelectrochemical methods will also be discussed later in this work. These methods can give information on thickness and optical constants of adsorbed layers, reaction kinetics, et cetera.

In spectroelectrochemistry there are two ways to study the surface of an electrode: in-situ, where the electrochemical cell would be in operation during the measurement, and ex-situ, where the electrode is removed from the cell for external examination. The in-situ method is a more applicable method for studying the electrode interphase than the ex-situ method because the in-situ method is able to monitor processes at the electrode interphase as they happen. In the ex-situ method, that is not possible. The ex-situ methods observe a change on the surface of the electrode before and after an electrochemical experiment is performed. Ex-situ methods can give a great deal of information, but are usually performed under ultra high vacuum. Thus the interphase changes a great deal and the information gained is much less revealing about the dynamic processes concerned. The ex-situ techniques are useful only in cases where there are simple systems involved, or strongly adsorbed molecules are present, since the environment of the molecules in the interphase necessarily changes a great deal in going from solution to vacuum. References pertaining to

in-situ and ex-situ methods are given in Table 1 and no further discussion of ex-situ methods will be given here.

TABLE 1

References for Spectroelectrochemical Methods

In-situ Spectroelectrochemical Methods	References
I) Specular reflectance	
A) Ultraviolet-Visible	8, 11, 19, 30-36
B) Infrared	1-6, 84-86
II) IRS (U.V.-Visible, IR)	9, 10, 12, 13, 17, 18, 24, 38-48
III) Ellipsometry	49-52
IV) Transmission (U.V.-Vis., IR)	
A) OTE	17, 18, 20, 22, 25-29, 37
B) OTTLE	17, 18, 20-22, 54
V) Raman spectroscopy	
A) Raman spectroscopy	55
B) Resonance Raman	56-60
C) SERS	16, 61-71
In-situ Non-optical Methods	
I) Electron spin resonance	72-74
II) Mossbauer spectroscopy	75-76
Ex-situ Methods	
I) Low energy electron diffraction (LEED)	77-80
II) Auger spectroscopy	79-80

1.3 Solution Free Measurements

The in-situ spectroelectrochemical methods can be divided into two primary areas: 1) the study of "solution free molecules" (molecules able to diffuse to the electrode, transfer an electron or electrons at the electrode and then diffuse away), and 2) the study of the double layer structure, including adsorbed species.

First I shall discuss the "solution free molecule" experiments. In the "solution free method" the main information obtained is the determination of electrochemical reaction mechanisms of homogeneous reactions which accompany charge transfer processes. This technique (which may use radiation in the ultraviolet, visible or infrared region) is usually nondestructive and the absorption of light by the electroactive species is much faster than the kinetics of a chemical reaction following an electron transfer. This makes it ideal for the study of reaction mechanisms. The absorption of light by only the electroactive species as a function of time can yield the type of mechanism involved. Since each possible mechanism has a different absorbance vs. time curve for each absorbing species (17-20), and the curve for each mechanism can be simulated by finite difference (81) and orthogonal collocation methods (82, 83), exact mechanistic details can be obtained. For reversible reactions, the absorbance vs. time curve can be used to determine diffusion coefficients (31) and extinction coefficients of intermediates (19), products, and reactants.

The early methods used were internal reflection spectroscopy (IRS) and transmission spectroscopy with optically transparent electrodes. The IRS technique (9, 10, 12, 13, 17, 18, 24, 38-48) was first applied to spectroelectrochemistry in 1966 (43). This method introduces the light beam through the backside of an optically transparent electrode at an angle, usually 10 degrees greater than the critical angle, and the light beam is totally reflected at the electrode solution interphase. Even though the optical beam is totally reflected there is still an evanescent electric field which penetrates into the interphase which can be absorbed by species in the interphase during electrochemical processes, thereby attenuating the incident beam. The penetration depth of this electric field is dependent on the optical constants of the solution and the wavelength of incident radiation. This depth is usually about a tenth of a wavelength of the incident radiation. Sensitivity of this technique can be increased by multiple reflections. One problem with this method is that during the absorbance vs. time measurement, there is only a finite penetration depth (2,000A in visible region). Therefore, one necessarily reaches a steady state quite fast due to the rate of change of diffusional processes slowing down close to the electrode.

Transmission spectroelectrochemistry (17, 18, 20, 22, 25-29, 37) uses optically transparent electrodes which are set up in such a way as to perform transmission spectroscopy on the electrogenerated species. The cell is designed in such a way that the electrolyte layer is much thicker than the diffusion layer adjacent to the electrode. These techniques can be used in the ultraviolet, visible

and infrared. The major problem with IRS and transmission spectroelectrochemical methods is obtaining an optically transparent material that makes a good electrode. Most of the optically transparent electrodes are made by chemical vapor deposition of a thin film (100-500Å) of platinum, silver, gold, tin oxide, or indium oxide on a substrate that is determined by the wavelength range of light used. These films generally have a resistance of 5-20 Ω /sq., except for germanium and carbon film electrodes which have a resistance of 2000-5000 Ω /sq. Such high resistances can cause a potential difference across the electrode surface. A good review of optically transparent electrodes is given by Kuwana and Heineman (20).

Modulated reflection spectroscopy is rapidly becoming the most popular technique used in spectroelectrochemistry. It can be used in the ultraviolet-visible (8, 11, 19, 30-36) and the infrared (1-6, 84-86) to monitor electroactive species in solution or at the surface of the electrode. The method calls for radiation to be passed through a solution, and subsequently reflected from the surface of the electrode at an angle that may range from 1.0 to near 90 degrees and then back through the solution and out of the cell. The electrode potential is simultaneously modulated across a region of interest, and the resulting modulated light signal is analyzed by deconvolution of the small A.C. signal due to the electrochemical processes from the background radiation. Deconvolution by phase sensitive detection and signal averaging may be utilized to obtain the desired spectrum.

In the infrared, special problems arise because almost all electrochemical solvents absorb strongly in this region. Thus, a very

thin layer of solution (5-20 μm) is formed between the electrode and the external cell window which minimizes effects due to solvent absorption. The actual technique will be discussed in more detail later.

The modulated reflection spectroscopic techniques are the most sensitive of all the spectroelectrochemical methods. By the use of phase sensitive detection, 10^{-17} moles/cm^2 can be detected and with signal averaging, kinetic characteristic times at the microsecond level can be determined (8).

In its simplest form, a modulated Fourier transform infrared reflectance method (4, 84-86) used to detect electroactive intermediates does not have the inherent sensitivity of the phase sensitiv- methods (1-3, 5, 6), or the ability to monitor reaction kinetics. However, the technique has much higher resolution and has the advantages of advanced data manipulation and signal averaging. In this method, one collects spectra at two different potentials, and then subtracts them. This yields a difference spectrum of the species between the two potentials. Since it is usually only possible to hold the potential where electron transfer is occurring for a short time to avoid the effects of irreversible reactions, the electrode potential must be modulated. Thus only a few spectra can be taken at each potential. Therefore the electrode potential must be modulated many times and the scans collected at each potential are averaged to improve the signal to noise ratio. Typically, scans can be collected as fast as 0.1 sec/scan at 16 cm^{-1} resolution, and 0.6 sec/scan at 4 cm^{-1} resolution. For "solution free species" the spectral

changes reflect vibrational changes of the molecule before and after electron transfer.

The only major problem of modulated reflection spectroscopy is the electroreflectance effect (18, 36, 87). This effect occurs when the surface electron structure of the metal electrode is perturbed by modulation of potential. This property is universal among metal electrodes. When a potential is applied to an electrode, the Fermi level of the electrode changes which in turn causes the electronic structure near the surface to change. The optical constants which are dependent on the electronic structure near the surface thus change. Since the reflectivity of the metal is dependent on the optical constants, the reflectivity is dependent on potential. Since radiation may also effect electron density, the electroreflectance effect is wavelength dependent. Since this effect has a small (relative reflectance 10^{-6}) magnitude in the infrared region, it has no consequence in this work.

In resonance Raman spectroelectrochemistry (56-60) a similar cell configuration is used. The excitation of the molecule is by a laser which is of a frequency that lies within the absorption band of the electrogenerated species. The laser is directed through the solution and reflected from the electrode surface, from which the Raman scattering is observed. The resonance Raman line is usually enhanced by a factor of 10^4-10^6 over normal Raman scattering, thus making it possible to observe very small quantities. This technique gives information of the molecular structure of the electrogenerated species, and also has been shown to be useful in determining reaction kinetics. The major disadvantage of this technique is that not all

vibrational bands are enhanced to the same extent. In fact only those bands that are associated with the electronic transition that was excited may be observed.

Finally, another widely used technique is that of optically transparent thin layer electrodes (OTTLE) (17, 18, 20-22, 54). An OTTLE cell is a metal grid (100-2000 wires/in. usually gold) sandwiched between two optically transparent windows (the type of window substrate depends on the spectral region of interest). The solution thickness is usually less than 0.2 mm. The OTTLE method is a transmission method which is mainly used for electrolysis experiments. Here, usually all of the electroactive species is electrolyzed in 20-120 sec. There are other uses, such as indirect coulometric titrations (22) with optical monitoring. Their small sample size makes them ideal for dealing with expensive biological molecules (53). An obvious drawback to this method is that the electrode is a grid instead of a planar electrode, thus making kinetic measurements at short times impossible due to the lack of accurate mathematical description of such systems (18).

The above methods of "solution free spectroelectrochemistry" may not be used alone to determine the actual mechanism and homogeneous rate constants of the relaxation of the electrogenerated species. Other electrochemical methods must be used first to determine at what potential the charge transfer occurs. A spectrum is then run to determine the wavelength where the electrogenerated species absorbs. Then it is possible to sit at the absorbing wavelength and monitor the absorbance vs. time curves necessary to

elucidate the reaction mechanism, extinction coefficients, and kinetics of the homogeneous reactions. In general, it is always good practice to use spectroelectrochemical techniques in conjunction with electrochemical techniques for determining reaction mechanisms.

1.4 Surface Studies

I will now look at other types of in-situ spectroelectrochemical methods which deal with the structure of the double layer and molecules adsorbed on the electrode.

The spectroelectrochemical method of ellipsometry (49-52) is used to determine the two optical constants and the thickness of films adsorbed on an electrode. When plane polarized light is specularly reflected from a surface, the reflected light will be polarized elliptically. The method for measuring the state of polarization of reflected light is called ellipsometry. Since this is an in-situ method, it can be used to determine kinetics of film formation and dissolution.

It was shown in 1980 (1) that Modulated Infrared Reflection Spectroscopy (MIRRS) (1-3, 5, 6) could be used to study the vibrational structure of the electrode/electrolyte interphase using phase sensitive detection. In this work it will been shown that Modulated Fourier Transform Infrared Reflection Spectroscopy (MFTIRRS) (4, 84, 86) can also be used to investigate the vibrational structure of the electrode/electrolyte interphase. The general techniques for obtaining MFTIRRS spectra were described previously. In addition, it is required

that the distance from the electrode to the window be less than 6 μm to minimize the solvent absorption. The infrared beam that is reflected from the electrode surface must be polarized parallel to the plane of incidence. The electrochemical cells for MIRRS and MFTIRRS are identical. Description of the cell will be made in a later chapter.

Another technique for studying vibrational structure of the electrode/electrolyte interphase is surface enhanced Raman spectroscopy (SERS) (16, 61-71). In this technique, a laser exciting beam is directed through solution and is reflected off the electrode back through the solution. The Raman backscattering is then detected normal to the electrode surface.

The in-situ vibrational spectroelectrochemical methods each have specific advantages. First, all of the techniques may show an enhancement of the signal as much as 10^6. The reasons for enhancement in SERS are not fully understood. There are many theories, such as surface plasmon excitation, surface roughness enhancement, and charge transfer complexes on the surface (16). Until the underlying reason for this enhancement is determined, the technique will not be fully exploited. The infrared techniques also show an enhancement, the cause of which will be explained in a later chapter.

Second, the cells used in SERS experiments are able to provide faster electrochemistry than those used in MIRRS and MFTIRRS, because the electrode is usually 2 mm from the window, allowing more uninhibited diffusion of the species. Third, the MIRRS and MFTIRRS can use almost any type of electrode, as long as it is not a blackbody absorber.

This is not true with SERS, where only silver, copper and gold electrodes will work.

Each of the vibrational spectroelectrochemical methods follow surface selection rules (88, 89) which specify that only molecules oriented in certain directions will absorb the incident radiation.

For infrared radiation the reason for this is that when s-polarized light is reflected from the surface, there is a phase shift of 180 degrees (for all angles of incidence) of the reflected beam with respect to the incident beam. The phase shift will cause a node at the surface, so that there is no electrical component of the radiation for the absorbed species to interact with. This is also true for p-polarized light at normal incidence. When p-polarized light is used, there is a phase shift of less than 180 degrees for all angles of incidence (except normal and 90 degree angles of incidence). This creates a standing wave on the surface with the electric vector component normal to the surface. This component reaches a maximum at about 88 degrees incidence (depending on the metal) then falls off rapidly to zero at 90 degrees incidence. There is thus energy available to interact with absorbed dipoles. In addition, it may be shown that only dipole oscillators with a non-zero component of the dipole derivative ($\partial\mu$ / ∂ Q) perpendicular to the surface will interact with the p-polarized radiation.

Vibrational data can give significant information on the structure and bonding characteristics of the molecules adsorbed or weakly interacting with the surface.

CHAPTER 2

EXPERIMENTAL

2.1 Preparations

2.1.1 Purification of Acetonitrile

Acetonitrile was the primary electrochemical solvent used in this work. The purfication of acetonitrile was accomplished by using a modified procedure of Mann et al (92). The impurities in commercial grade acetonitrile may include unsaturated nitriles, acetamide, ammonium acetate, acetic acid, aldehydes, amines, ammonia and water. Since these impurities are electroactive they must be removed to achieve proper electrochemical behavior of this solvent. 2.5 liters of commercial grade acetonitrile was distilled rapidly over a short Vigreux column discarding the first and last 100 ml collected. The middle fraction (2.3 liters) was collected over 10 gm of calcium hydride, and was allowed to stand for 24 hrs. This first part of the procedure removed a large amount of the impurities, including almost all of the water. In the next part, which removes aromatic hydrocarbons, no more than 0.2% water can be present. The solvent was decanted from the calcium hydride into a flask containing 25 ml of benzoyl chloride. The mixture was refluxed for 1 hour, then distilled (5 ml/min.) into a flask containing 25 ml of H_2O to hydrolyze any benzoyl chloride carried over. This was followed by discarding the

last 100 ml of distillate. The middle fraction was distilled again, this time discarding the first 50 ml and last 100 ml of the distillate. Then to the distillate, 25 gm of potassium permanganate were added. The mixture was distilled rapidly, discarding the first and last 50 ml of the distillate. The receiving flask was fitted with a drying tube to keep atmospheric water out. The distillate was made acidic with concentrated sulfuric acid to precipitate any ammonium sulphate out of solution. Any ammonia present was formed in the previous step. The solution was then decanted from the ammonium sulphate, then distilled (10 ml/min.) into a flask containing 25 gm of calcium hydride. The first and last 50 ml were discarded. The final distillation was performed in a carefully dried distillation apparatus containing a four foot insulated column packed with glass helices. The distillate containing the calcium hydride was distilled (1 ml/min.) under a dry argon atmosphere, discarding the first 50 ml and last 100 ml. This final purified acetonitrile was stored over Woelm super grade alumina under a dry argon atmosphere until use.

The purification procedure yields about 60% of the starting material. The dry purified acetonitrile shows an absorbance of less than 0.5 for a 1-cm cell at 200 nm. The electrochemistry of the product had a steady state background current of less than 50 $\mu A/cm^2$ at +3.00 V vs. Ag/Ag^+ (0.01M) reference electrode, with (0.1 M) tetra-n-butylammonium tetrafluoroborate as the supporting electrolyte. The above small background current can only be achieved if all the glassware is very dry. This usually calls for Woelm super grade

alumina to be added to the electrochemical cell to remove the last traces of water.

It has also been found that Caledon HPLC grade acetonitrile with 0.006% water could be used as is after drying over Woelm super grade alumina.

2.1.2 Preparation of Tetra-n-butylammonium Tetrafluoroborate

Tetra-n-butylammonium tetrafluoroborate was prepared by a modified method of Lund and Iverson (93). 100g of sodium tetrafluoroborate was dissolved in a minimum amount of distilled water and filtered. Similarly, 340 gm of tetra-n-butylammonium hydrogen sulfate was dissolved in a minimum amount of distilled water and filtered. The $NaBF_4$ solution was added slowly with stirring to the tetra-n-butylammonium hydrogen sulfate solution. The tetra-n-butylammonium tetrafluoroborate precipitated out of solution immediately, and was then filtered and washed with two 100 ml portions of ice cold distilled water. The precipitate was dissolved in 75 ml of methylene chloride. The mixture was transferred to a separatory funnel and shaken. The mixture formed two immiscible layers, the lower layer methylene chloride plus tetra-n-butylammonium tetrafluoroborate, and the upper layer water and sodium bisulphate. The lower layer was added to 300 ml of ice cold diethylether with vigorous stirring. The tetra-n-butylammonium tetrafluoroborate precipitated out of solution slowly. After about 15 min. the precipitate was filtered and dried under vacuum at 80°C for 72 hours.

2.1.3 Purification of Commercial Chemicals

Benzophenone (Fisher Scientific) was recrystallized twice from 98% ethanol and vacuum dried at 40°C (94).

Tetracyanoethylene (Eastman) was recrystallized from chlorobenzene twice, and vacuum dried at 50°C (95).

Tetra-n-butylammonium perchlorate (Fluka) was dissolved in a minimum amount of acetone. It was precipitated by adding doubly distilled water. This procedure was repeated twice. The final precipitate was dried under vacuum at 50°C (96).

Lithium perchlorate (Thiokol) was recrystallized from triply distilled water twice. The final precipitate was dried under vacuum at 100°C (97).

Anthracene puriss (Aldrich 99.9%) was used as received.

2.2 Optical Cell and Electrodes

The infrared spectroelectrochemical cell used is of the three electrode type, with platinum working and secondary electrodes and a Ag/Ag^+ (0.01M) reference electrode. The cell is shown in Figure 1. It was made out of pyrex glass, and had an overall length of 175 mm with the working electrode inserted. About 75 ml of solution was needed to fill the cell. When the mirror working electrode was placed in the cell, it was pushed forward until the electrode surface was against the optical window. The luggin capillary tip was mounted 0.5 mm from the optical window and 3 mm below the working electrode.

IR-ELECTROCHEMICAL CELL

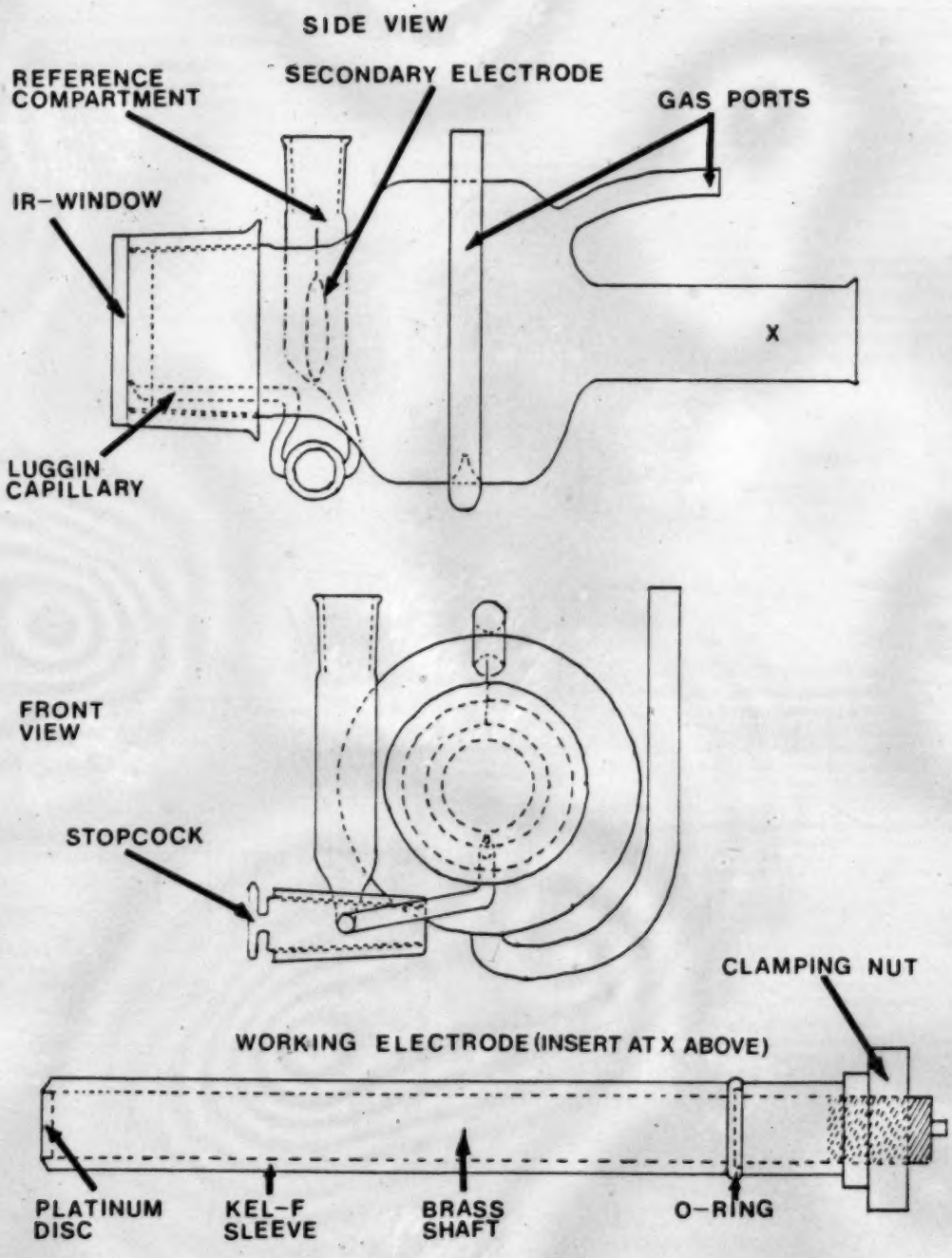

FIGURE 1

A loosely fitting ground glass stopcock was used to connect the Luggin tube with the reference compartment, and it served to isolate the two compartments. The secondary electrode was an 18 gauge platinum wire loop around the working electrode shaft, and was parallel to the optical window. When the cell was purged with dry argon, use was made of two special ports. These ports were mounted at the top and bottom of the main cell body.

The working electrodes were made by silver soldering a 2 mm x 12 mm (dia.) platinum disk to a 12 mm x 175 mm brass rod. The first 135 mm of the brass rod (containing the platinum disk) was press fitted into a 3 mm thick Kel-F sleeve. The Kel-F sleeve was press fitted by heating the sleeve and pressing it on to the epoxy resin coated brass rod. This procedure produced a seal which was resistant to organic solvents and acids. At the rear of the electrode was another Kel-F sleeve of the same O.D., but this sleeve was made to slide on and off. A rubber O-ring was placed between the two Kel-F sleeves. The rear end of the brass rod was threaded and a plastic nut was screwed on the end. The nut was used to apply pressure on the rear sleeve which in turn expanded the O-ring which served as a seal when the electrode was placed in the cell. There was approximately 0.1 to 0.2 mm of clearance between the O.D. of the working electrode and the I.D. of the cell. This clearance was made minimal to maintain the electrode shaft perpendicular to the optical window.

The electrode was polished by mounting it in an aluminum mandril shown in Figure 2. The mandril was used to maintain the electrode face perpendicular to the electrode shaft. The two screws on the

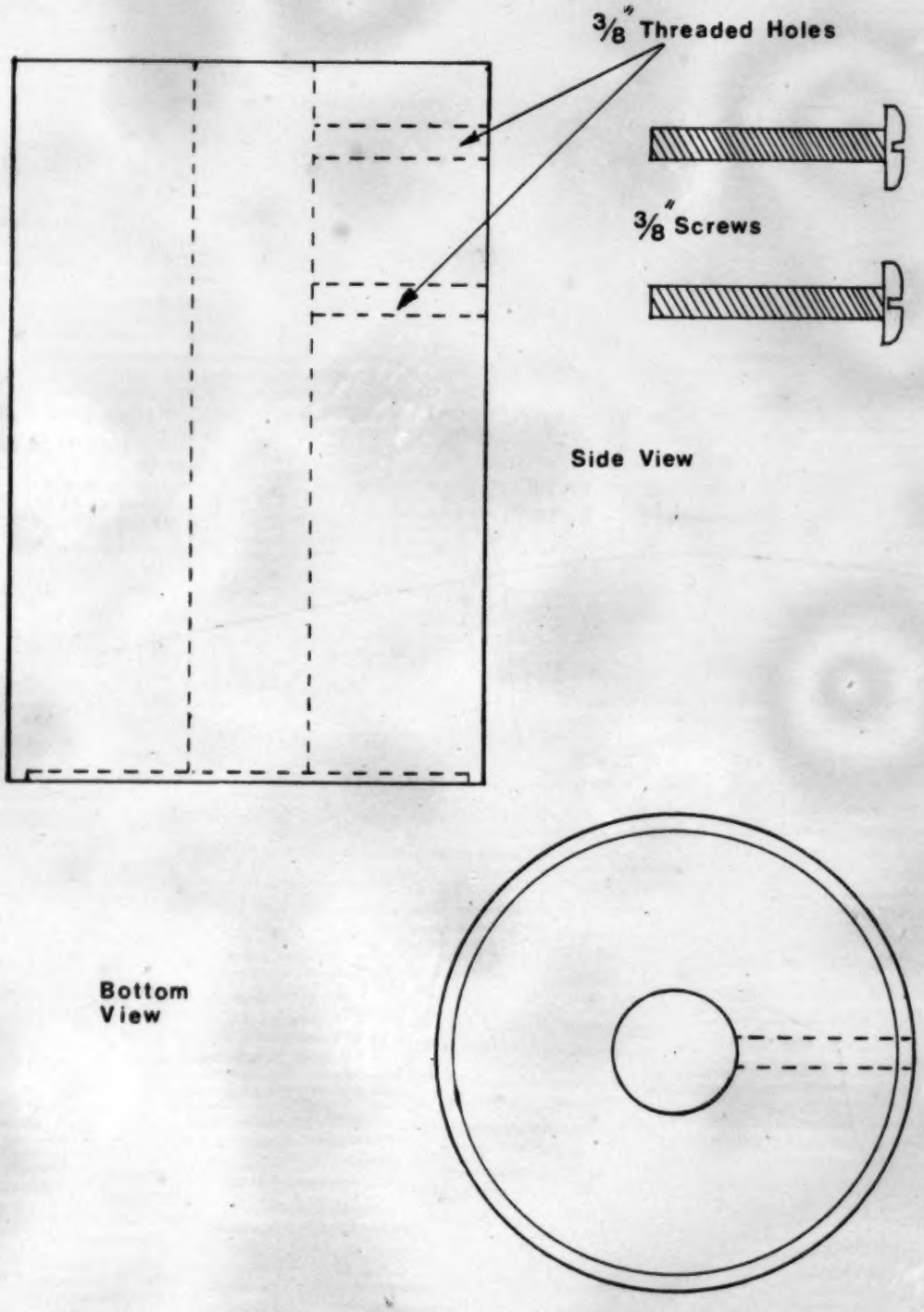

Figure 2. Polishing mandril for the mirror working electrode.

side of the mandril were used to tighten the electrode in place while polishing. A polishing pad (Buehler) was stretched and bonded to an 8" square piece of plate glass. The sequence of polishes used for polishing the electrode started with 1.0μm polishing alumina (Baikalox), then 0.3 μmand finally with 0.05μm polishing alumina. Each polishing was performed with the aid of distilled water.

The optical windows chosen were zinc sulfide and zinc selenide. These windows are resistant to organic solvents, weak acids, and water. Zinc sulfide is transparent from 14,000 cm^{-1} to 650 cm^{-1} and has an index of refraction of 2.25 at 2000 cm^{-1}. Zinc selenide was transparent from 20,000 cm^{-1} to 400 cm^{-1} and had an index of refraction of 2.4 at 2000 cm^{-1}. Both of the windows (35 mm dia. x 2 mm thick) were mounted on a ℨ 34 female ground glass joint with epoxy resin. Before they were mounted on a glass joint, the joint was cut so that the face of the joint was perpendicular to the working electrode shaft. The face was also cut in such a way that when it was mounted on the cell, the height of the face was only 0.5 mm above the Luggin capillary.

The determination of the distance between the electrode surface and the optical window was accomplished in three steps. First, by the use of Beer's Law, the total pathlength of the incident and reflected beams between the electrode and the window was determined. This is shown pictorially in Figure 3. Beer's Law is given by:

$$A = \varepsilon bc \qquad (1)$$

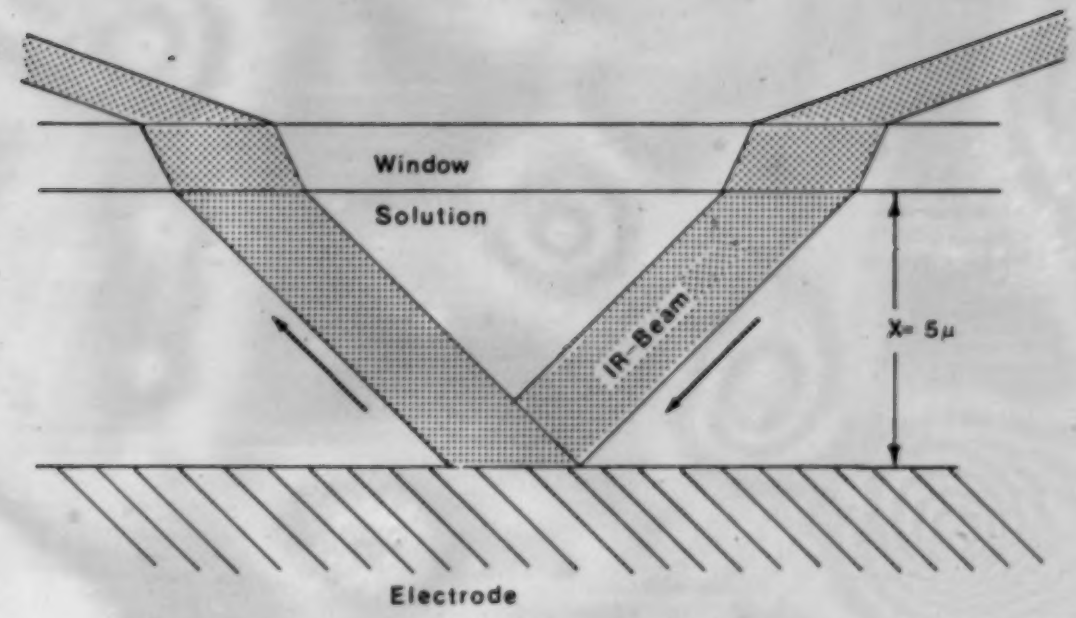

Figure 3. The path of the infrared beam through the cell.

where A is the integrated absorbance of the entire band, ε is the integrated molar absorptivity, C is the molar concentration and b is the optical pathlength in centimeters.

To avoid error due to deviations from Beer's Law a standard measurement was made with the same resolution (4 cm^{-1}) and concentration as was used with the reflectance cell. Two bands of acetonitrile, the C-C stretch, $\bar{\nu}_4$ (921 cm^{-1}) and the $-CH_2$ antisymmetric rock, $\bar{\nu}_7$ (1040 cm^{-1}) were used in the Beer's Law calculation. Three standard spectra were made with acetonitrile in a freshly prepared 0.05 mm solution cell. For each spectrum the absorbance was integrated over the entire band for both of the vibrations $\bar{\nu}_4$ and $\bar{\nu}_7$. By using equation (1) the integrated molar absorptivity was calculated as 309 $\pm$ 2 and 78 $\pm$ .5 for $\bar{\nu}_7$ and $\bar{\nu}_4$ respectively. Two more spectra were taken, but this time the light beam was reflected through the reflectance cell filled with acetonitrile. Before the second spectrum was taken the electrode was pulled back and then pushed up against the window to determine the reproducibility of the gap between the electrode and the window. As before, the absorbance was integrated over the entire band for both of the vibrations $\bar{\nu}_4$ and $\bar{\nu}_7$. By using equation (1) the total optical pathlength was determined to be 1.5×10^{-3} and 1.6×10^{-3} centimeters for the first and second runs respectively.

In the second step, the angle of incidence of the infrared beam to the electrode surface was determined. Snell's Law predicts the angle at which light is refracted when going from one medium to another

with different index of refraction and is stated as:

$$n_1 \sin i = n_2 \sin R \qquad (2)$$

The terms n_1 and n_2 are the indices of refraction of the first and second media respectively, i is the angle of incidence, and R is the angle of refraction. The media zinc sulfide, acetonitrile, and air have indices of refraction of 2.25, 1.34, and 1.00 respectively (lit.). The angle of incidence on the cell window was 70 degrees. Thus from equation (2) the angle of incidence to the electrode surface was found to be 45 degrees

The final step was to determine the distance between the electrode surface and the optical window from the equation:

$$x = \frac{\Gamma \cos \Theta}{2} \qquad (3)$$

The term Γ is the total optical pathlength, Θ is the angle of incidence to the electrode surface, and x is the distance between the electrode and the window. By applying equation (3) the distance between the electrode and the window was determined to be 5.3 μm and 5.7 μm for the first and second measurements respectively. These values show that the distance between the electrode and the window was reasonably reproducible. This small thickness was only used when studying surface processes. A much thicker distance was used when studying electroactive species. In this latter case the solution thickness was also reproducible because the electrode was pulled back from the window until the band at 1449 cm^{-1} had an absorbance of 1.0. This correlated to a thickness of about 20 μm. At this thickness none of the acetonitrile

bands were so strong that they would fully block out any region in the spectrum. Larger thicknesses began to present sensitivity problems.

2.3 Instrumentation

2.3.1 Spectrometer

The instrument used in this study was a Nicolet 7199 Fourier transform infrared spectrometer. An interferometer was chosen instead of a dispersive spectrometer because of the optical and digital advantages that the interferometer had to offer. This is the first work in which an interferometer has been used to study the in-situ electrode interphase. Previous work in this area has been done with dispersive spectrometers with phase sensitive detection (1-3,5,6). A detailed explanation of the operation of the interferometer system is given elsewhere (98,99). The basic mode of operation of the interferometer was to convert the information at infrared frequencies to lower audio frequencies and phase relate these frequencies so that the detectors and the electronics are able to follow both frequency and intensity information of the infrared radiation.

A simplified diagram of the Nicolet 7199 spectrometer is shown in figure 4. The Michelson interferometer consisted of two planar mirrors perpendicular to each other; one was fixed in place and the other was moved back and forth at a constant velocity of 0.783 cm/sec. The interferometer also had a germanium beam splitter on a KBr substrate and a KBr compensator.

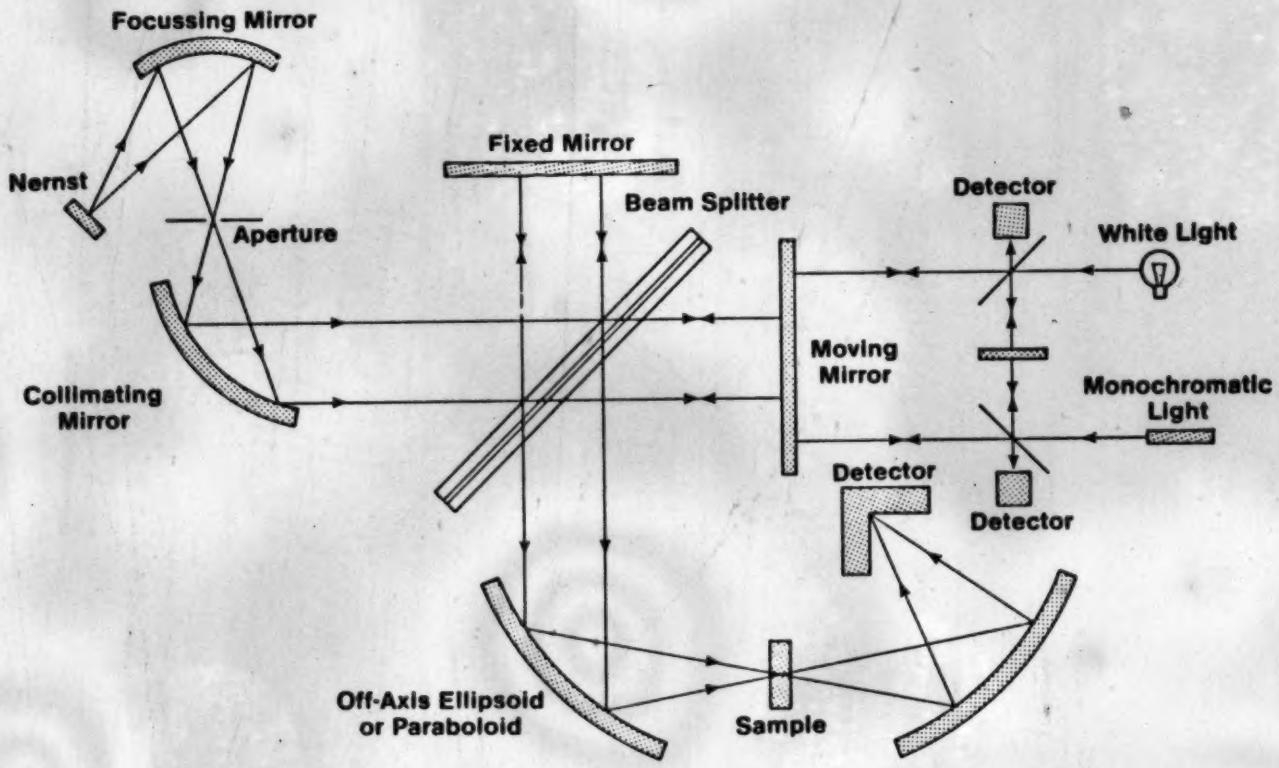

Figure 4. Simplified diagram of the Nicolet 7199 spectrometer.

The beamsplitter was placed at 45 degrees to the fixed and movable mirrors. An infrared beam (collimated) was directed on to the beamsplitter and ideally 50 percent was reflected to the fixed mirror and 50 percent was transmitted to the moving mirror. The infrared light beam was collimated by focusing the light from the source, a water cooled globar, onto a 0.250 in. aperture. The aperture was placed at the focal length of a spherical mirror which produced a light beam of high enough collimation to achieve $0.3 cm^{-1}$ resolution from the instrument.

If collimated monochromatic light of wavelength λ cm is directed into the interferometer it will be split at the beamsplitter into two beams of equal intensity. One beam will be directed to the fixed mirror and the other to the moving mirror. The beams will be reflected by these mirrors back to the beamsplitter where they will be recombined. If the pathlengths of the two mirrors to the beamsplitter are the same (this is known as zero retardation) the two beams will be in phase and will constructively add. Thus ideally the detector will see the total intensity of the source.

If the movable mirror is retarded $\lambda/2$ cm from zero retardation, the two beams will be 180° degrees out of phase and interfere destructively. Thus no light will reach the detector as it is all reflected back to the source.

For monochromatic light, the output of the interferometer produces a cosine wave as the movable mirror is displaced. This cosine wave is also called an interferogram and is shown in Figure 5. The signal has a maximum intensity at integral multiples of λ cm retarda-

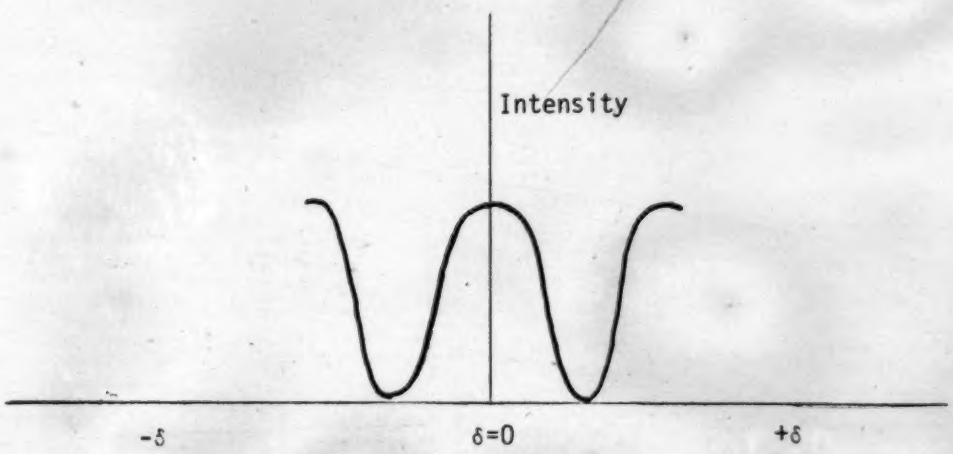

Figure 5. Cosine wave interferogram.

tion, and a minimum intensity at integral multiples of $\lambda/2$cm retardation. The intensity at the detector for a monochromatic source, as a function of mirror retardation is given by

$$I'\{\delta\}=0.5I\{\nu\}\ (1+\cos\ 2\ \pi\nu\delta) \qquad (1)$$

where δ is the mirror retardation, and $I(\nu)$ is the intensity of the source. This expression has two components, a modulated component given by $0.5I\{\nu\}\cos\ 2\pi\nu\delta$ and a constant component given by $0.5\ I\{\nu\}$. In this study only the modulated component need be considered. Thus the equation is simplified to

$$I\{\delta\}=\ 0.5I\{\nu\}\cos\ 2\ \pi\nu\delta \qquad (2)$$

Since the interferometer used in this study was not ideal, a frequency dependent correction factor was added. The correction is needed because of beamsplitter efficiency, detector response, and amplifier characteristics which are all frequency dependent. Therefore, equation (2) is modified by the correction factor which is given by

$$I\{\delta\}=\ 0.5H\{\nu\}I\{\nu\}\cdot\cos 2\pi\nu\delta \qquad (3)$$

Equation 3 is simplified by letting $B(\nu)$ be equal to $0.5H\{\nu\}I\{\nu\}$. where $B(\nu)$ is the intensity of the source after it has been changed by the instrumental characteristics. $I(\delta)$ is then given by $I\{\delta\}=B\{\nu\}\cos 2\pi\nu\delta$ (4)

When the movable mirror is moving at a constant velocity, a monochromatic source of wavenumber ν produces an interferogram that is a cosine wave of a specific frequency. Thus the frequency of the cosine wave is given by

$$f=2V\nu \qquad (5)$$

where f is in Hertz, V is the velocity of the mirror in cm/sec, and ν

is the wavenumber of the monochromatic source in cm^{-1}.

If the source emits more than one wavelength of light, the detector will respond to the sum of all the cosine waves. Thus the interferogram of a polychromatic source is given by

$$I\{\delta\} = \int_{-\infty}^{\infty} B\{\nu\} \cos 2\pi\nu\delta \, d\nu \qquad (6)$$

A typical interferogram of an infrared source is shown in Figure 6. Equation 6 is one half of a cosine Fourier transform pair, the other being

$$B\{\nu\} = \int_{-\infty}^{\infty} I\{\delta\} \cos 2\pi\nu\delta \, d\delta \qquad (7)$$

Equations 6 and 7 represent the relationship between the interferogram and the spectrum.

In practice it is physically impossible to retard the movable mirror from positive to negative infinity. Thus only a finite resolution is possible. The resolution of the interferometer is given by

$$\Delta\nu = \{\Delta \text{ cm}\}^{-1} \qquad (8)$$

where Δ in cm is the maximum mirror retardation from zero retardation, and $\Delta\nu$ is the nominal resolution. In this study the mirror was moved 0.250 cm from zero retardation, thus the maximum resolution possible was 4 cm^{-1}. Since the interferometer is limited to a finite mirror movement Δ, this is the same as multiplying the interferogram by a truncation function. The cosine Fourier transform of an infinitely long cosine wave gives a spectrum with one infinitesimally narrow spike at wavenumber ν. When the cosine Fourier transform is applied to a truncated cosine wave the calculated spectrum is also one line at wavenumber ν but the line is of lower resolution. The spectrum for the truncated interferogram has an instrument line shape

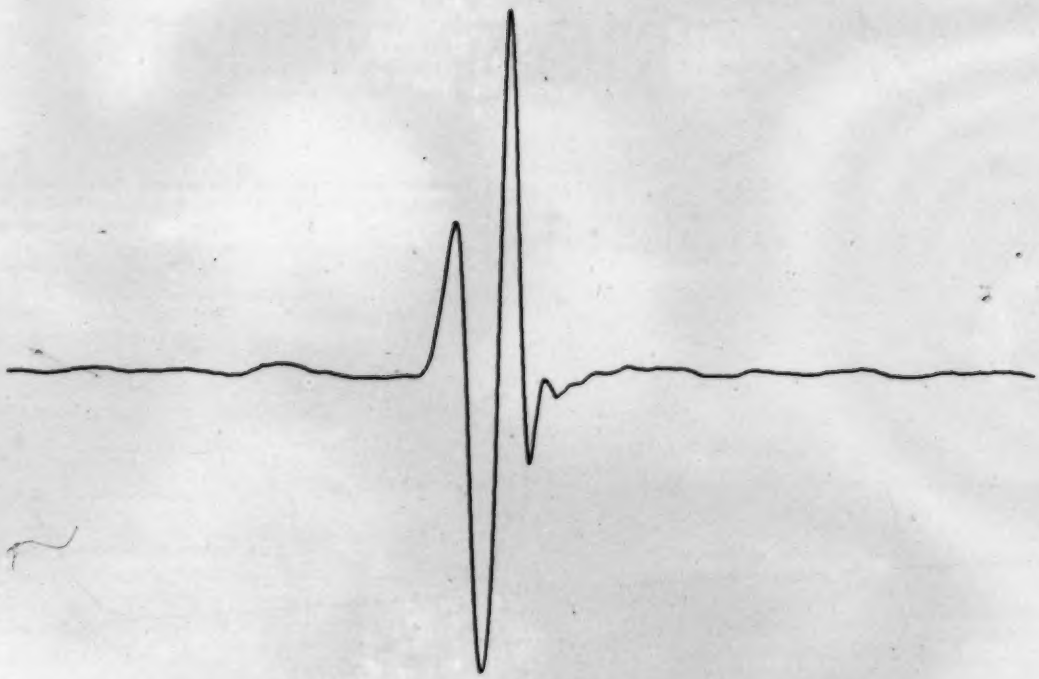

Figure 6. Typical mid infrared interferogram.

function sin X/X, as shown in figure 7. In that figure, the full width at half height is $0.605/\Delta\ cm^{-1}$ and the band has a peak height of 2Δ. The full width at half height is used to define the instrument resolution. The sin X/X instrument line shape generates side lobes initially at 20% of the central peak height. This produces difficulties in finding bands of low intensity close to the central peak. To remove or reduce these side lobes a method called apodization is used. This method calls for multiplying an interferogram by an apodization function $H(\delta)$. Thus the spectrum is given by

$$B\{\nu\}= \int_{\infty}^{\infty} I\delta\} H\{\delta\}\cos 2\pi\nu\delta \, d\delta \qquad (9)$$

In this study the apodization function used was the Happ-Genzel function given by

$$H\{\delta\}=0.54 + 0.46\ \pi\delta\ \Delta \qquad \Delta<\delta<+\Delta$$

$$H\{\delta\}=0 \qquad \delta<-\Delta,\ \delta>\Delta$$

The calculated spectrum using the Happ-Genzel apodization gave an instrument line shape $h(\nu)$ (100)

$$h\{\nu\}= \left(0.54/\pi\nu+(0.46\cdot 4\pi\nu\Delta^2)/(\pi^2 -(2\pi\nu\Delta)^2)\right)\sin 2\ \pi\nu\Delta \qquad (10)$$

This instrument line shape has a width at half peak height of 0.91 $\Delta^{-1} cm^{-1}$ and a peak height of 1.08Δ. The side lobes are only produced in the spectrum when the width of the spectral line is

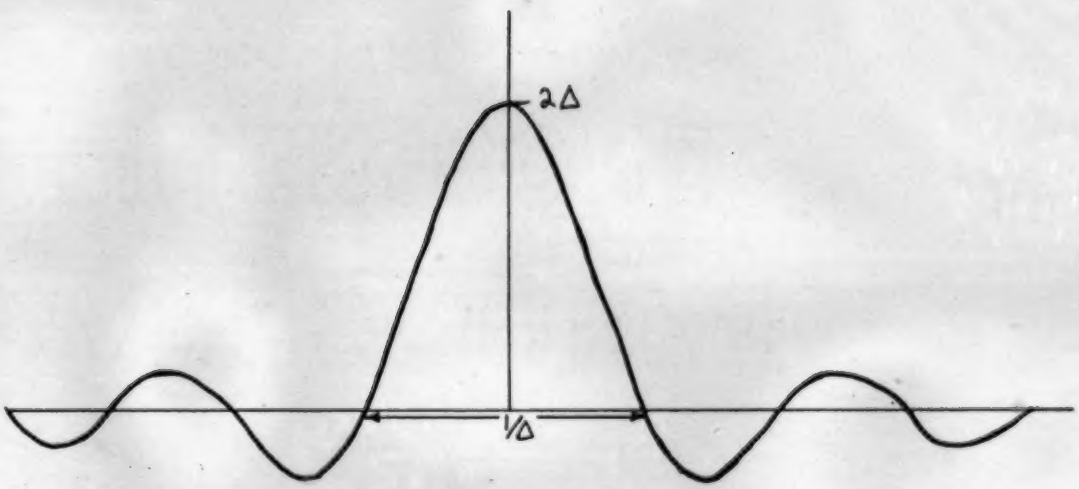

Figure 7. Instrument line shape: the function sin x/x.

less than the resolution of the instrument Δ^{-1}, because otherwise the spectral information encoded in the modulation of an interferogram has faded to zero in the sampled part of the interferogram.

In practice there is a problem in obtaining a proper spectrum from an interferogram due to phase error. The phase error is caused by optical, electronic, and sampling effects. Most of these may be frequency dependent. To eliminate these effects, a correction factor is added. Thus the interferogram becomes

$$I\{\delta\}=\int_{-\infty}^{\infty}B\{\nu\}\cos\{2\pi\nu\{\delta+X\{\nu\}\}\} \tag{12}$$

Since a cosine wave may be represented as:

$$\cos(A+B) = \cos A \cdot \cos B - \sin A \cdot \sin B \tag{13}$$

we have

$$I\{\delta\}=\int_{-\infty}^{\infty}B\{\nu\}\cos 2\pi\nu\delta 2\cos\pi\nu X\{\nu\}-B\{\nu\}\sin\pi\nu\delta 2\cdot\sin 2\pi\nu X\{\nu\} \tag{14}$$

Equation 14 shows that by adding a correction factor, sine components are added to the interferogram. The cosine Fourier transform of the interferogram $I(\delta)$ is given by (100)

$$C\{\nu'\} =\int_{-\infty}^{\infty}I\{\delta\}\cos 2\pi\nu'\delta\ d\delta \tag{15}$$

The sine Fourier transform of the interferogram $I(\delta)$ is given by (100).

$$S\{\nu'\} =\int_{-\infty}^{\infty}I\{\delta\}\sin 2\pi\nu'\delta\ d\delta \tag{16}$$

The method of removing the sine component is called phase correction. In the Nicolet spectrometer used in this work, phase correction of the spectra was performed in the following manner: the interferogram that was collected by the spectrometer was single sided, except for a few hundred points collected on the opposite side of zero retardation. The computer calculated a phase spectrum by transforming part of the interferogram that contained 100 points on both sides zero retardation. The sine and the cosine Fourier transforms (98) were calculated from this double sided interferogram, and the phase spectrum $\theta(\nu')$ was given by

$$\theta(\nu')=\arctan S'(\nu')/C'(\nu') \qquad (17)$$

The sine and cosine Fourier transforms (98) were then computed from the total single sided interferogram, and the real phase corrected single beam spectrum was determined by using the following relation

$$B(\nu')=C(\nu')\cos\theta(\nu')+ S(\nu')\sin\theta(\nu') \qquad (18)$$

The interferogram was sampled by using the interferogram of a He-Ne laser. Since the interferogram of a laser is a cosine wave, the output of the laser detector was electronically converted into a square wave and used to trigger the A/D converter to record the output of the infrared detector. In this work a data point was taken once every laser wavelength and the frequency of the laser was 15798 cm^{-1}. Thus by using the Nyquist theorem the highest possible frequency that may be sampled without aliasing is 7899 cm^{-1}, which is also known as the bandwidth. Frequencies higher than this are optically and electronically filtered out. Since the laser frequency is precise, it

gives rise to accurate distance measurements of the movable mirror, which in turn gives rise to accurate infrared frequencies. The infrared frequencies produced by the Nicolet spectrometer are accurate to 0.1 cm^{-1}.

Before an interferogram was transformed it was usually averaged many times. Thus it was necessary to start the averaging at the same point. This was done with an electronic pulse that was produced from the interferogram of a white light, which was optically offset to produce this pulse approximately 1000 data points before the zero retardation of the infrared interferogram.

The ratio of the signal to noise increases with the square root of the number of scans, if the detector is noise limited, and is given by (101)

$$S/N = B(t,\nu)\Theta n\Delta\nu tm^{\frac{1}{2}}/NEP \qquad (19)$$

where $B(t,\nu)$ is the intensity of the source as a function of temperature and frequency, Θ is the optical throughput, n is the overall efficiency, $\Delta\nu$ is the instrument resolution, tm is the observation time for each spectral element, and NEP is the noise equivalent power of the detector.

The interferometer has many advantages over the dispersive spectrometer such as Fellgett's advantage (98,99,102), Jacquinots's advantage (98,99,102), and digital advantages produced by the data handling abilities of a computer.

Fellgett's or the multiplex advantage is the ability of an interferometer to view all the spectral resolution elements at once. The number of spectral elements is given by

$$M=\upsilon_b/\ \Delta\nu \tag{20}$$

where υ is the bandwidth of the spectrum, and ν is the instrument resolution. If a dispersive spectrometer only measures one spectral element at a time, we know an interferometer can collect a spectrum M times faster or have a signal to noise ratio $M^{\frac{1}{2}}$ times greater than the dispersive instrument. Jacquinot's advantage is known as the throughput advantage. This one may be of no benefit to us in the far infrared, since with a dispersive spectrometer one has the ability to switch to gratings of higher efficiency at longer wavelengths. The Jacquinot's advantage is given by

$$\Theta_I/\ \Theta_G=2\ \pi A_I f a\nu^2/A_G h\ \upsilon_B \tag{21}$$

where Θ_I is the optical throughput of the interferometer, υ_b is the bandwidth, A_I is the area of the mirrors in the interferometer, Θ_G is the optical throughput of the dispersive instrument, h is the height of the slits, f is the focal length used to collimate the light, and a is the line spacing of the grating.

2.4 Apparatus

A modified Harrick retro-reflectance attachment was mounted in the back beam of the Nicolet 7199 spectrometer. The reflectance attachment was modified by removing one mirror and replacing it with the electrochemical reflectance cell, and the mirror mount for the removed mirror was lowered so that the mirror working electrode was mounted in the center of the infrared beam. The basic apparatus is shown in figure 8. The electrochemical reflectance cell was mounted in a cell holder shown in figure 9.

The infrared beam was incident on the cell window at an angle of 60 to 70 degrees, or approximately the Brewster angle of the cell window. The infrared beam was polarized with a gold wire grid polarizer on a barium fluoride substrate (Cambridge Physical Sciences type IGP228) after it was reflected from the cell. The polarizer was set to let only the radiation component parallel to the plane of incidence be transmitted. The component of the electric field vector polarized perpendicular to the plane of incidence has a node at the surface, thus it is not absorbed by surface species. The signal to noise ratio can be increased by a factor of 2 by removing the s-polarized component, since this component contains no information of interest and only contributes to the saturation of the detector or A/D converter.

The detector used in the Nicolet 7199 spectrometer was a mercury-cadmium-telluride photoconductive solid state unit, with a specific detectivity D* of approximately 1×10^{10} cm $H_z^{\frac{1}{2}}/W$.

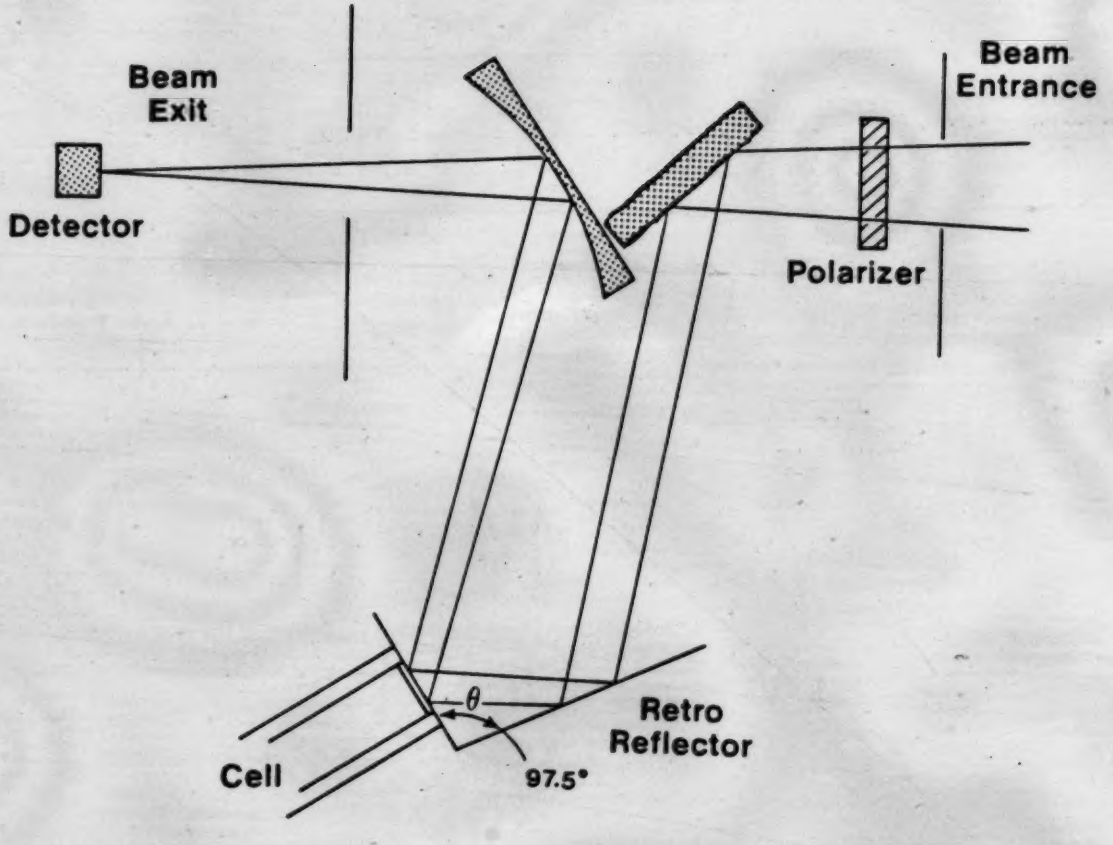

Figure 8. Installation of reflection apparatus in sample compartment of spectrometer.

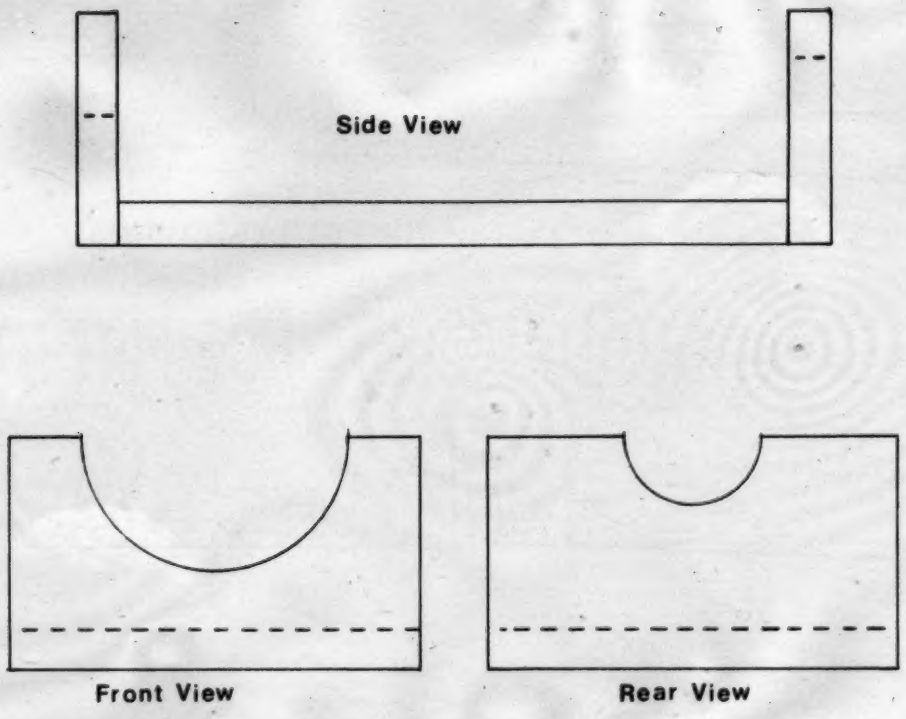

Figure 9. Electrochemical reflectance cell holder.

The potential of the working mirror electrode was controlled by a Hi-Tek Instruments DT2101 potentiostat that was driven by a Hi-Tek Instruments PPR1 waveform generator. The potentiostat was triggered by the spectrometer's computer by tapping the output of the "sweep" BNC connector located on the back of the computer. The computer gave a TTL pulse every time the computer started to collect a scan. A 74193 counter was used in the counting circuit that was connected in the triggering circuit between the sweep BNC connector and the potentiostat. The circuit for the counter is shown in Figure 10. The counter was used so that a series of scans could be collected at two different potentials. A scan is one interferogram collected, and usually more than one is collected at each potential so they are signal averaged as they are collected to increase the signal to noise ratio.

2.5 Data Collection

In this section, I will describe the complete procedure to collect a spectrum. The particular data collection procedure described first is that for studying the double layer. The computer was programmed to perform a collection routine and the potentiostat was triggered by a digital counter which counted the number of scans. It was also possible to trigger the potentiostat in sequence with the collection program. The language was Nicolet assembler.

The counter circuit designed for this study was a 4-bit modulo-16 down counter. The output of the third bit was connected to the "start" TTL input of the PPRI waveform generator.

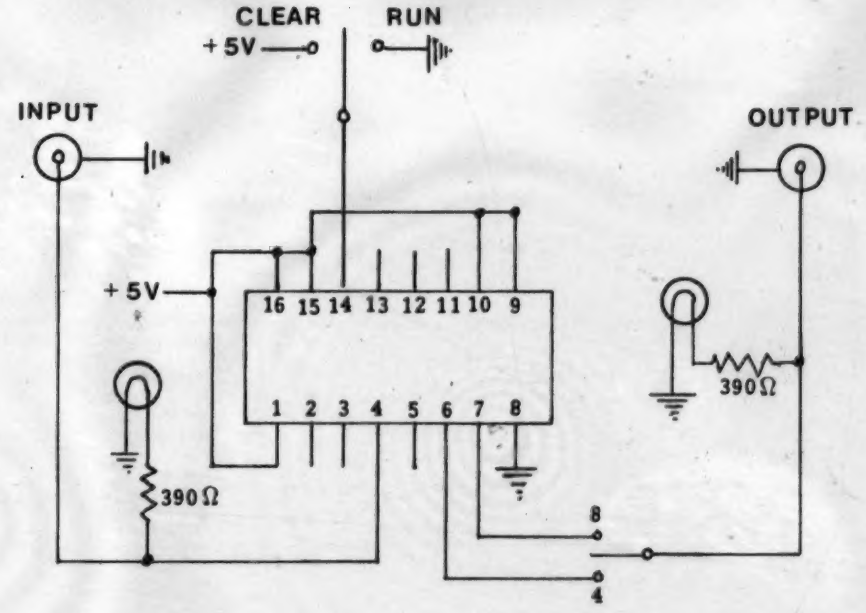

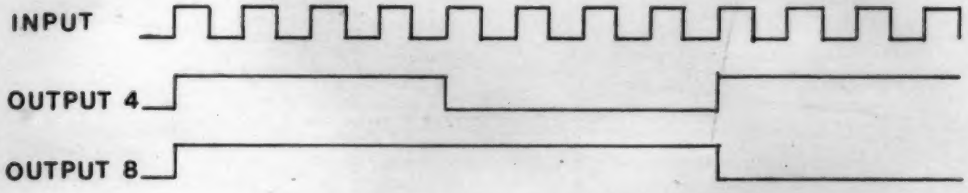

Figure 10. Counter Circuit

The base potential was set on the potentiostat and the potential step that would be applied was set on the waveform generator. The counter initially was set to make output of the third bit Lo. A command was given to the computer to collect four scans and store the average in a destination file number 20. The start of the first scan would make the third bit Hi, thus triggering the waveform generator which in turn triggered the potentiostat to apply the step potential to the working electrode. The waveform generator could only be triggered on $0 \rightarrow 1$ pulses. The third bit gave a $0 \rightarrow 1$ pulse output on the start of the first scan , since the counter was clocked with $0 \rightarrow 1$ pulses from the sweep BNC connector from the computer. The third bit of the counter would not give another $0 \rightarrow 1$ pulse to the waveform generator until after it received eight clock pulses (or until after eight scans had been taken). On the ninth pulse the counter would give another $0 \rightarrow 1$ pulse to the waveform generator, and thus apply the potential step to the working electrode. The length of time the potential step was applied was controlled by the waveform generator. It was set long enough to collect 4 scans in approximately 4 sec at 4 cm^{-1} resolution. After the working electrode was returned back to the base potential, a delay period of about twenty seconds was allowed before four more scans were collected at the base potential and the average was stored in the destination file number 21. The delay period was needed to let the system relax back to its original state.

The collection program 1 is listed in the appendix. The program provided for the collection of four spectra at the base potential and the storage of their average in a sample file. Subsequently, four

spectra were collected at the step potential and their average stored in the reference file. The interferogram in the sample file was added with a weighting factor to a sample interferogram previously stored in the destination file number 21. The interferogram in the reference file was also added with a weighting factor to a reference interferogram previously stored in the destination file number 20. The program contained a do-loop which displayed the sample file thirty times, corresponding to a planned delay of twenty seconds. The above sequence was nested in another do-loop, so that the sequence could be repeated N times. Therefore, 4N scans were collected in each of the destination files 20 and 21, corresponding to the step potential and the base potential respectively.

The collection program 1 could be changed to collect other numbers of scans at each potential by taking the output of the counter at other bits instead of the third bit. The same procedure given above would be used to collect the data.

The interferogram stored in the destination file number 20 was moved to the reference file and the interferogram stored in the destination file number 21 was moved to the sample file. The interferograms stored in the sample and reference files were then Fourier transformed, apodized, and phase corrected. The single beam spectra were then ratioed against a background ([sample/background] x 100 and [reference/background] x 100). Both spectra stored in the sample and reference files were changed from percent transmission to absorbance. The reference spectrum was then subtracted from the sample spectrum. The background was a single beam spectrum of the light

reflected through the reflectance attachment, and an empty reflectance cell. The infrared light was polarized parallel to the plane of incidence.

The spectrum resulting from subtraction is called a difference absorbance spectrum. The difference absorbance spectrum means that its base line has a zero absorbance and absorption bands extending below the zero line are due to species absorbing more strongly at the step potential than at the base potential. The absorption bands with an absorbance greater than the zero line are due to species absorbing more strongly at the base potential than at the step potential.

If there is a shift in the frequency of an absorption band at the base potential from that at the step potential, or the absorption band is broader at one potential than the other, bands in the resulting difference absorption spectrum may take on many different shapes. The shape of the difference absorption band depended on the relative intensities of the bands in the base potential spectrum and the step potential spectrum which were stored in the sample and reference files respectively. Some of the many different shapes that the difference adsorption band can assume are shown in Figures 11-13.

A slightly different collection routine was used for observing the infrared spectra of electrogenerated "solution free species". The "solution free species" are formed by oxidizing or reducing an electroactive species.

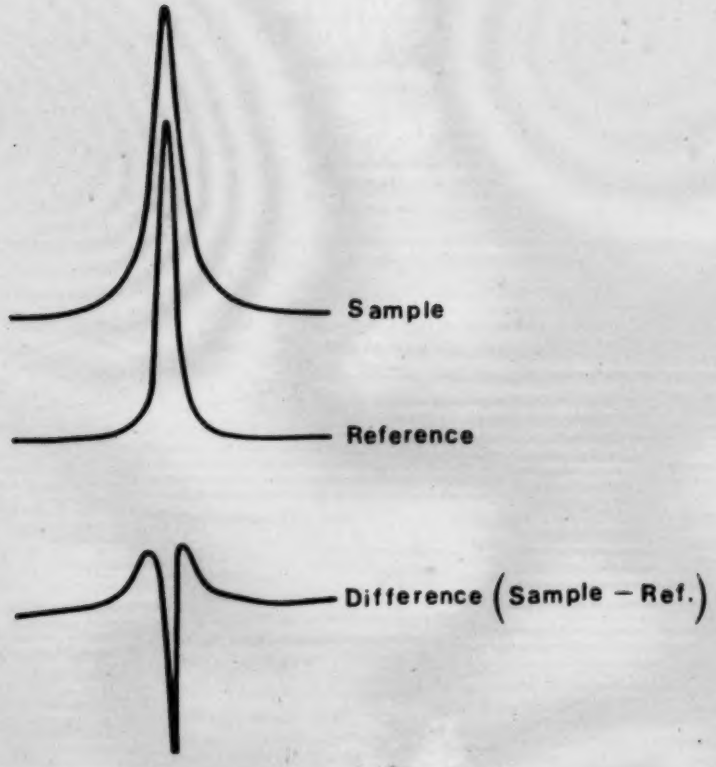

Figure 11. Difference absorption band type I.

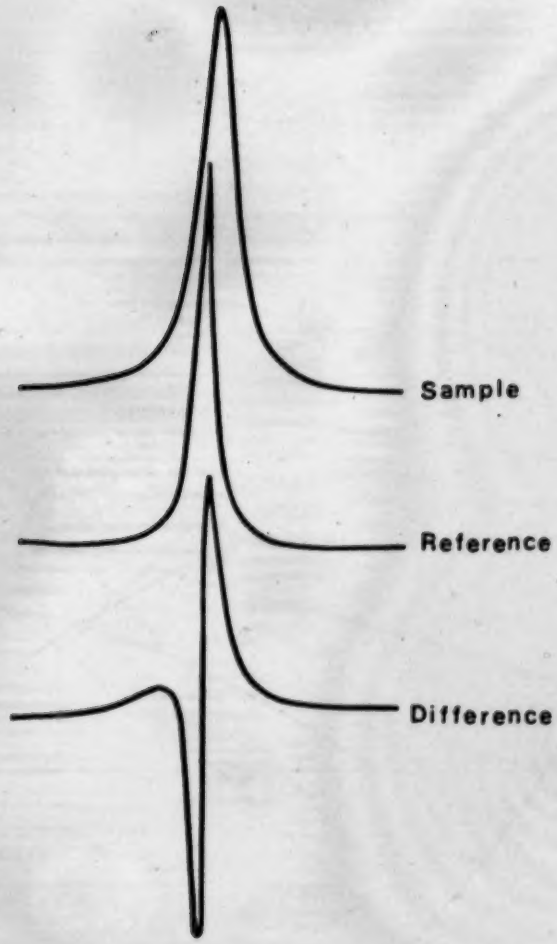

Figure 12. Difference absorption band type II.

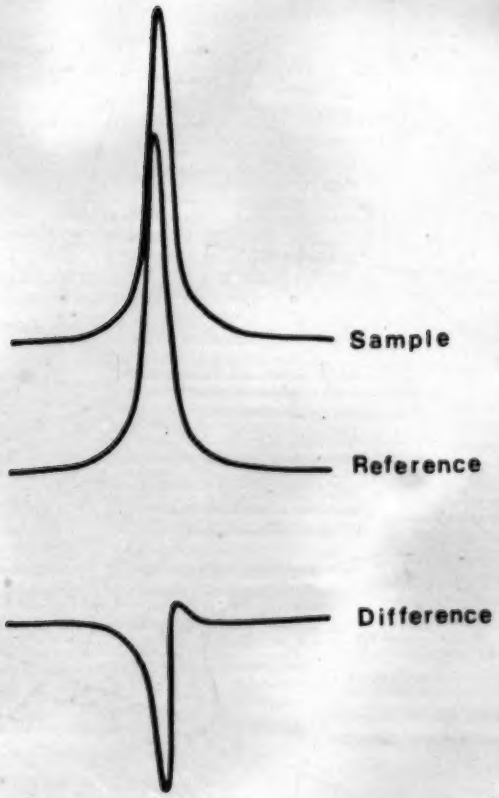

Figure 13. Difference absorption band type III.

A cyclic voltammogram was made to determine the peak potential where the electroactive compound is reduced or oxidized on the forward potential sweep and the peak potential where the electroactive compound was oxidized or reduced back to the neutral compound on the backward potential sweep. The base potential was set approximately 400 mV past the peak potential on the backward sweep of the oxidation or reduction back to the neutral compound, to insure that the reaction was diffusion controlled. The step potential was set approximately 200 mV past the peak potential on the forward sweep of the oxidation or reduction of the compound to insure that it also was diffusion controlled.

The base potential and the step potential were set on the potentiostat and the waveform generator respectively. Virtually the same procedure was used as before to collect the differential absorbance spectra. The counter was reset and four scans were collected at the step potential and the average was stored in the destination file number 18. After the potential returned to the base potential a twenty second delay was used before 4 scans were collected at the base potential and the average was stored in the destination file number 19. The delay was used to allow enough time for all the oxidized or reduced species to be reduced or oxidized back to the neutral species. Four more scans were then collected at the step potential and the average was stored in the destination file number 17. This collection also set the counter in the right position to start the collection program 2.

The collection program 2 is slightly different from the collection program 1 by virtue of having an extra collection file. The extra collection file was used to act as a delay to allow time for more of the reduced or oxidized species to be formed. Figure 14 shows how the concentration of the oxidized or the reduced form of the electroactive compound changes with time. The delay was approximately 3 seconds which was usually long enough to oxidize or reduce most of the electroactive compound in the thin solution layer between the mirror working electrode and the window. Thus the more material formed, the greater the amount of light absorbed by the compound, and thus the better the signal to noise ratio. The collection program 2 is listed in the appendix. The program first instructed a collection of four scans at the base potential and stored the average in the sample file. Then two scans were collected at the step potential and the average stored in the background file. With the potential step still being applied two more scans were collected and the average stored in the reference file. The interferogram stored in the sample file was added with weighting to the previously stored interferogram in the destination file number 19. The interferogram stored in the background file was added with weighting to the previously stored interferogram in the destination file number 18. The interferogram stored in the reference file was added with weighting to the previously stored interferogram in the destination file number 17. Then a do-loop was used which displayed the sample file 30 times giving a 20 second delay. The above sequence was nested in a do-loop and was repeated N times which gave 4N scans at the base potential and 4N scans at the step potential. The same triggering

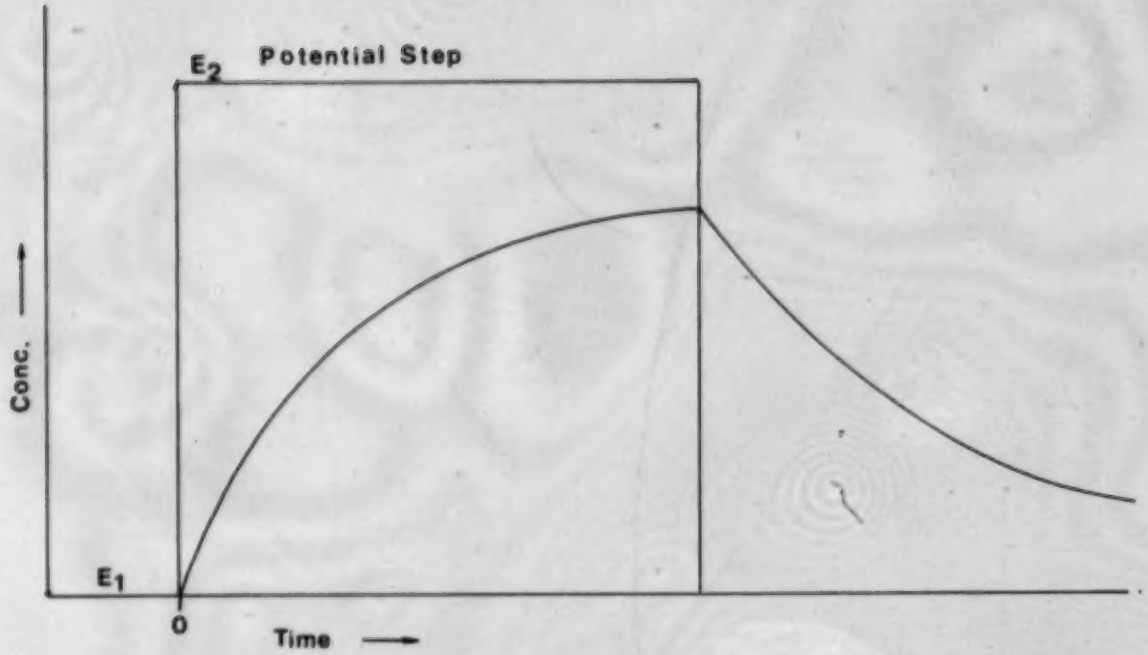

Figure 14. Concentration profile of electrogenerated species vs. time.

sequence was used in program 2 as used in program 1, because there was still four scans being collected at the base potential and four scans collected at the step potential, except now the scans taken at the step potential were stored in two different files. The interferogram stored in the destination file number 19 was moved to the sample file and the interferogram stored in the destination file number 17 was moved to the reference file. The two interferograms stored in the sample and reference files were Fourier transformed, apodized, and phase corrected. The single beam spectra stored in the sample and reference files were ratioed against the same background that was used before. The spectra stored in the sample and reference files were changed from percent transmittance to absorbance and subtracted, using the same method as before. The resulting difference absorbance spectrum had absorption bands above and below the zero absorbance base line. The absorption bands above the base line were due to a decrease in the absorption of neutral species. The absorption bands below the base line were due only to the electrogenerated species. If absorption bands didn't change in going from the neutral species to the elecrogenerated species, those absorption bands would not be observed in the difference absorbance spectrum.

3.0 Double Layer Structure

3.1 Results

Infrared difference spectra of a 0.1 M solution of tetrabutylammonium tetrafluoroborate in anhydrous acetonitrile at various potential steps are shown in Figure 15. The line drawn through each spectrum refers to the zero baseline. Absorption bands extending below the baseline correspond to an increase in the absorption of radiation at the step potential with respect to the absorbance at the base potential. The opposite is true for bands extending above the baseline. Table 2 lists the absorption band frequencies for the spectra shown in Figure 15. The base potential of each spectrum was -0.50 V *vs* Ag/Ag^+ reference electrode. That base potential was chosen because of its vicinity to the point of zero charge (PZC) of platinum in acetonitrile with the electrolytes used (106). The positive limit of the potential steps was governed by the solvent breakdown; thus the usable range was -2.0 V to + 2.5V vs Ag/Ag^+ reference electrode. The above solution was made 0.1 M in water and the resulting difference spectra are shown in Figure 16. The absorption band frequencies for Figure 16 are listed in Table 3. Difference spectra from the same experiment performed on an anhydrous acetonitrile solution of 0.1M lithium perchlorate are shown in Figure 17 and the absorption band frequencies are listed in Table 4. Figure 18 gives the corresponding spectra produced after 200 μl water was added to the 100 ml of lithium perchlorate solution and the absorption

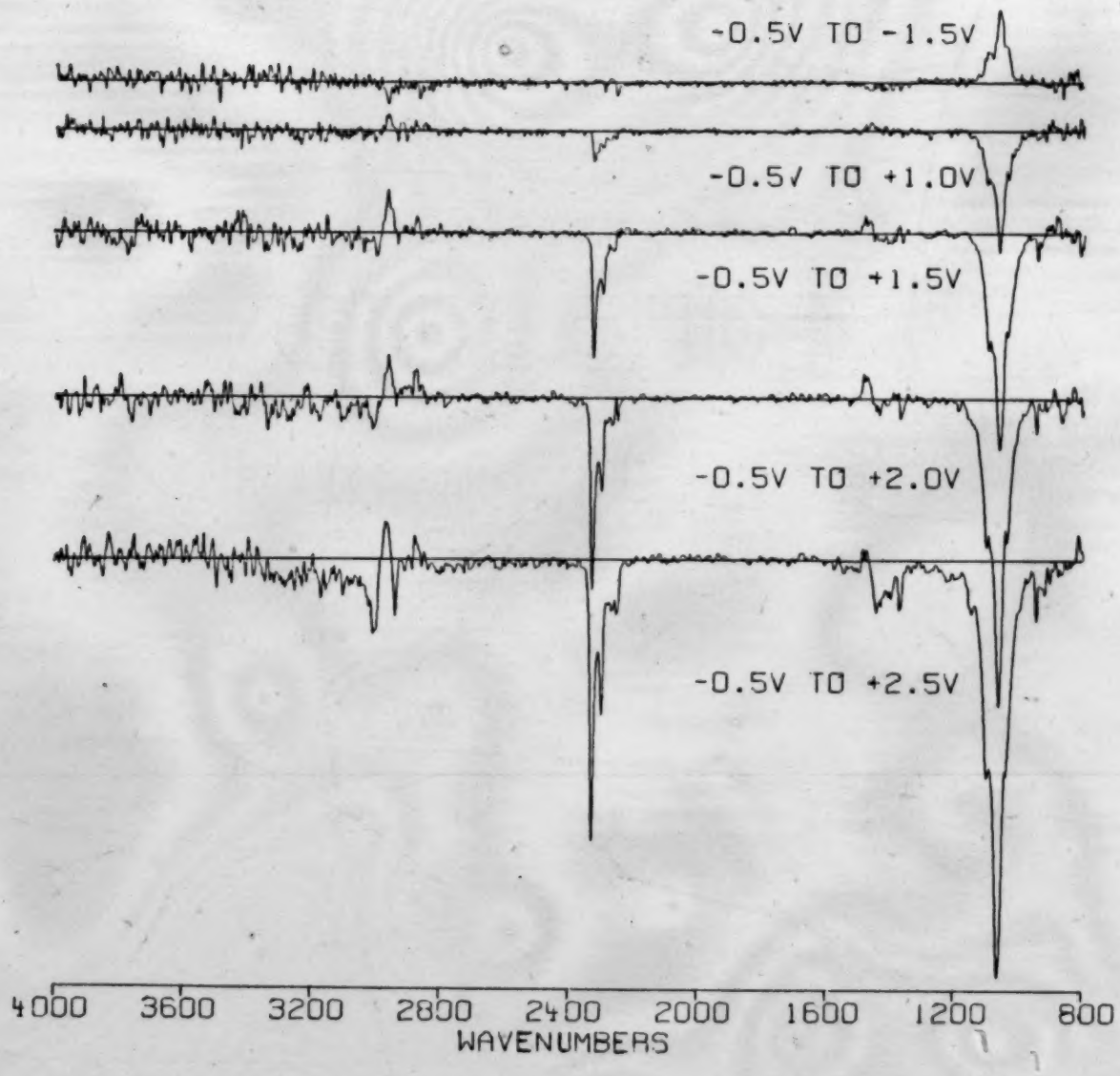

Figure 15. Difference spectra of 0.1M tetrabutylammonium tetrafluoroborate in acetonitrile. Platinum electrode.

Table 2

Band positions/cm^{-1} for difference spectra of 0.1 M tetrabutylammonium tetrafluoroborate in acetonitrile (dry)

Potential step	Pos. displaced bands	Neg. displaced band
-0.5V to +1.0V	2969 w 1470 vw	3005 vw 2938 vw 2328 m 2299 w 1100 m 1065 s 1035 m
-0.5V to -1.5V	2971 m 2881 vw 1480 w	3005 vw 2940 vw 2329 s 2300 m 2250 vw 1420 vw 1367 vw 1099 s 1065 vs 1038 s 948 w
-0.5V to +2.0V	2967 m 2880 w 1478 w	3010 w 2940 vw 2329 s 2298 m 2250 w 1425 vw 1365 w 1100 s 1065 vs 1039 s 946 w
-0.5V to +2.5V	2971 m 2881 w 1475 vw	3006 m 2942 m 2329 vs 2300 s 2255 m

Table 2 (Continued)

Band positions/cm^{-1} for difference spectra of 0.1 M tetrabutylammonium tetrafluoroborate in acetonitrile (dry)

Potential step	Pos. displaced bands	Neg. displaced band
		1420 w 1370 w 1100 s 1064 vs 948 m 920 vw
-0.5V to -1.5V	1064 s	2970 m

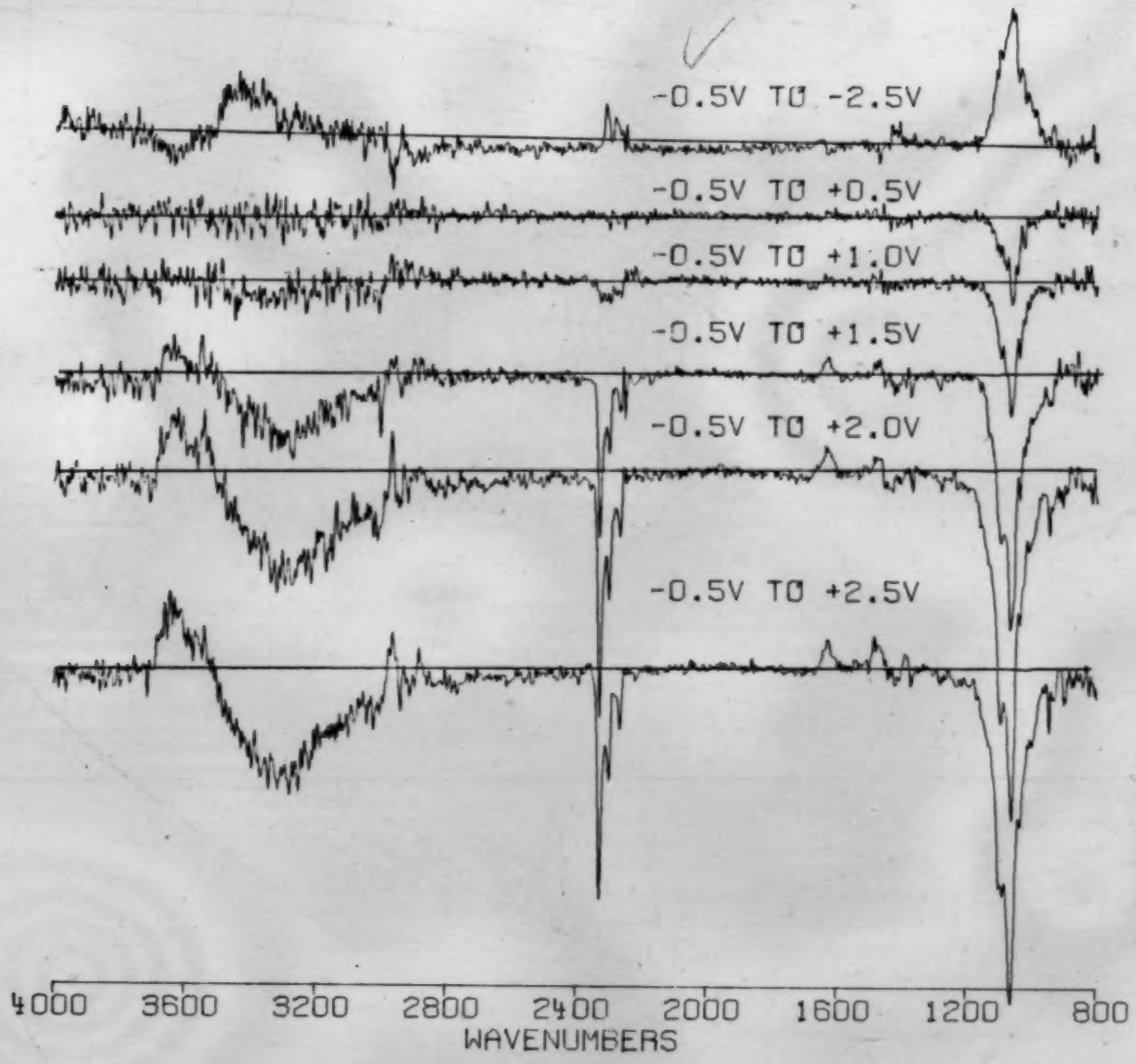

Figure 16. Difference spectra of 0.1M tetrabutylammonium tetrafluoroborate and 0.1 M water in acetonitrile. Platinum electrode.

Table 3

Band positions/cm^{-1} for difference spectra of 0.1 M tetrabutylammonium tetrafluoroborate and 0.1 M water in acetonitrile

Potential step	Pos. displaced bands	Neg. displaced band
-0.5V to -2.0V	3450 m (broad) 2315 m 2287 w 1660 vw 1425 w 1063 s	3640 w 3550 w 2971 m 1625 m
-0.5V to +0.5V		1063 s
-0.5V to +1.0V	2235 vw	2310 w 2265 vw 1670 vw 1063 s
-0.5V to +1.5V	3640 w (broad) 3545 w 2965 vw 1628 w	3300 w (broad) 3002 m 2940 w 2329 s 2302 m 2265 w 1680 vw 1420 vw 1375 vw 1095 s 1064 vs
-0.5V to +2.0V	3635 m 3545 w 2967 m 1633 w 1470 vw	3320 m (broad) 3006 w 2942 w 2329 s 2301 m 2265 m 1700 vw 1094 vs 1064 vs 947 w

Table 3 (Continued)

Band positions/cm^{-1} for difference spectra of 0.1 M tetrabutylammonium tetrafluoroborate and 0.1 M water in acetonitrile

Potential step	Pos. displaced bands	Neg. displaced band
-0.5V to +2.5V	3635 m 3550 w 2966 w 2884 w 1626 w 1486 w	3320 m (broad) 2941 w 2329 s 2301 m 2266 m 1680 vw 1095 s 1064 vs 950 m

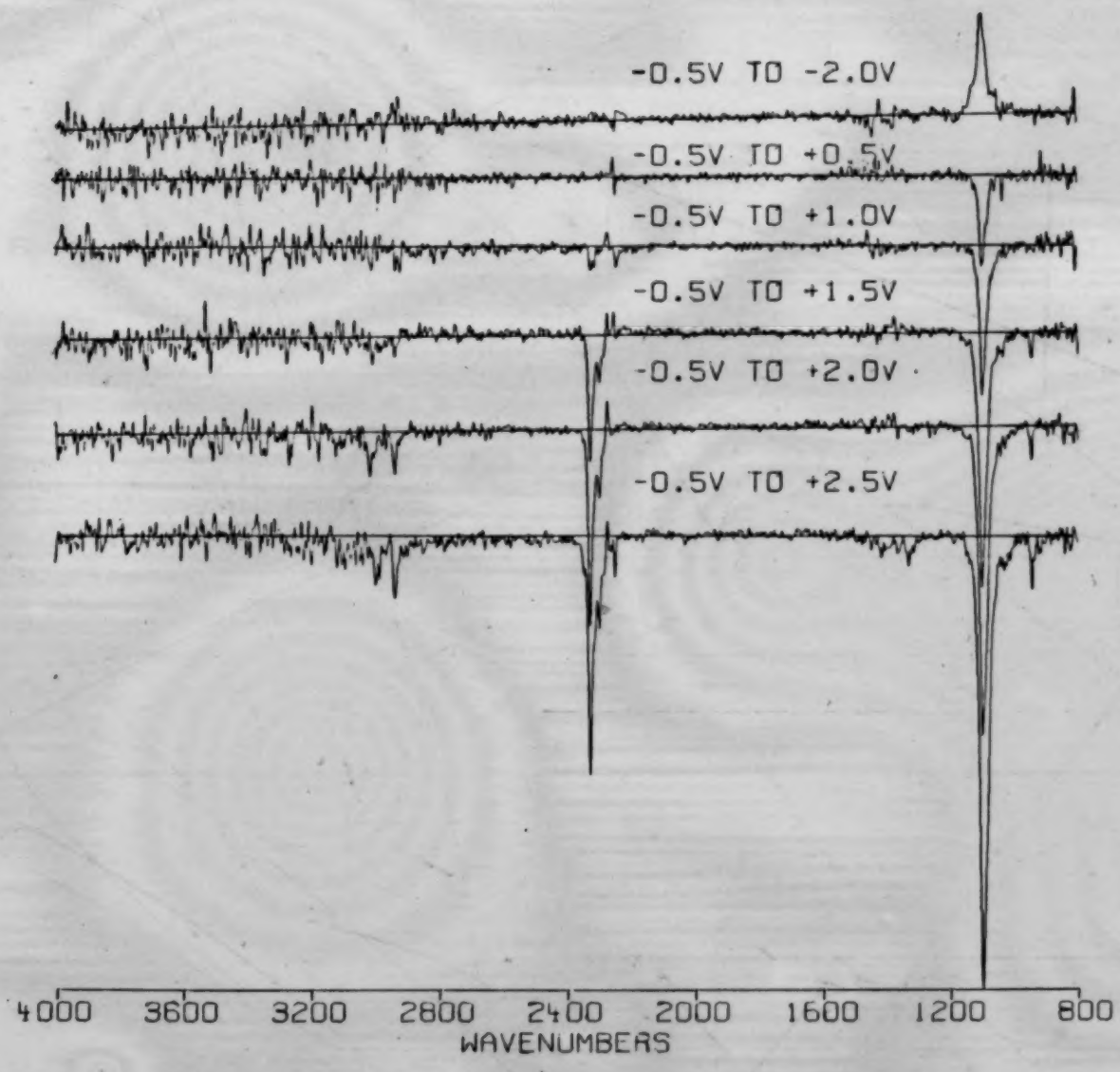

Figure 17. Difference spectra of 0.1M lithium perchlorate in acetonitrile.

Table 4

Band positions/cm^{-1} for difference spectra of 0.1 M lithium perchlorate in acetonitrile (dry)

Potential step	Pos. displaced bands	Neg. displaced band
-0.5V to -2.0V	1420 w (broad) 1100 w	1443 vw
-0.5V to +0.5V		1100 s
-0.5V to +1.0V	2270 w 1460 w	2325 w 2250 w 1102 vs
-0.5V to +1.V	2275 w 2250 w	3005 vw 2939 vw 2329 s 2300 m 1102 vs 948 w
-0.5V to +2.0V	2273 vw	3016 m 2939 m 2329 s 2300 m 1102 vs 948 m
-0.5V to +2.5V	2274 w	3000 w 2937 w 2329 s 2301 m 2250 w 1102 vs 948 m

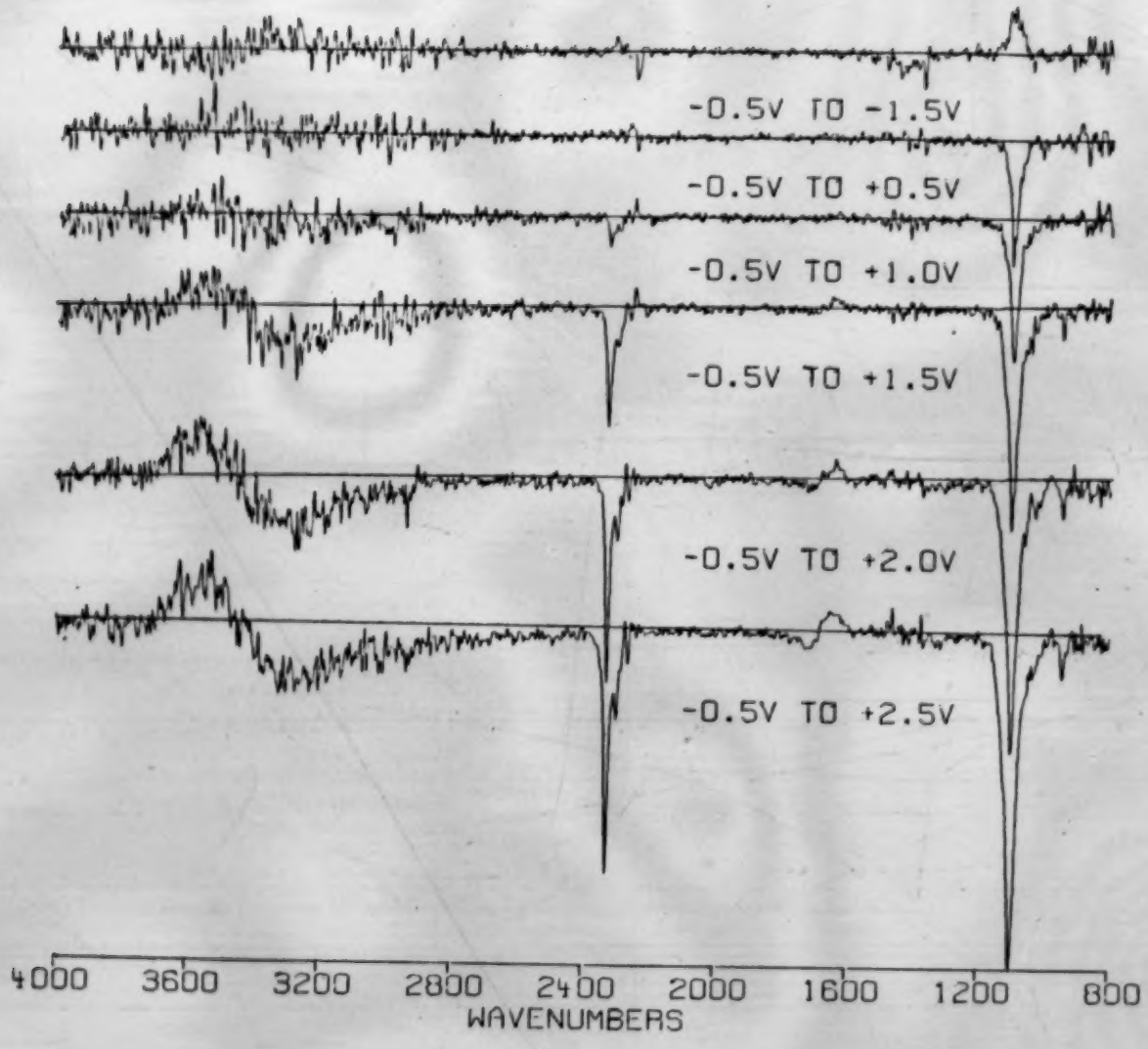

Figure 18. Difference spectra of 0.1M lithium perchlorate and 0.1M water in acetonitrile.

band frequencies are listed in Table 5.

The electrolyte was changed to 0.1M lithium hexafluoroarsenate in anhydrous acetonitrile and the same experiment was performed again. Figure 19 gives the corresponding spectra produced and the absorption band frequencies are listed in Table 6.

The mirror working electrode was changed from platinum to gold. The potential step experiment was performed with 0.1M lithium perchlorate in acetonitrile with 0.006% water and the resulting difference spectra are given in Figure 20. The absorption band frequencies of the spectra in Figure 20 are given in Table 7.

The infrared spectrum of anhydrous acetonitrile is given in Figure 21. The band frequencies and assignments are given in Table 8.

The infrared spectra of lithium perchlorate, lithium hexafluorarsenate, and tetrabutylammonium tetrafluoroborate are given in Figures 22,23 and 24 respectively. Listings of the bands of those spectra are given in Table 9.

3.2 Discussion

The difference spectra of the potential step experiments quite clearly exhibit changes with potential. The changes are a result of the interaction of the solution with the electrode at various potentials. Only reversible processes occurring in the thin layer of solution between the electrode and the window were monitored with the potential step experiment. We find that the resulting

Table 5

Band positions/cm^{-1} for difference spectra of 0.1 M lithium perchlorate and 0.1 M water in acetonitrile

Potential step	Pos. displaced bands	Neg. displaced band
-0.5V to -1.5V	1100 m	
-0.5V to +0.5V		1103 s
-0.5V to +1.0V	2275 vw 2253 w	1099 s
-0.5V t +1.5V	3620 vw 3550 vw 3460 vw 2251 w 1635 vw	3350 w 2329 s 2264 m 1700 vw 1102 vs 948 w
-0.5V to +2.0V	3630 w 3560 w 2275 vw 2254 vw 1638 w	3320 m (broad) 2941 w 2329 s 2300 m 1700 vw 1103 vs 948 m
-0.5V to +2.5V	3625 w 3540 w 1648 w 1463 vw 1377 vw	3340 m 3010 vw 2940 vw 2329 s 2300 m 2265 w 1715 w 1101 vs 946 m

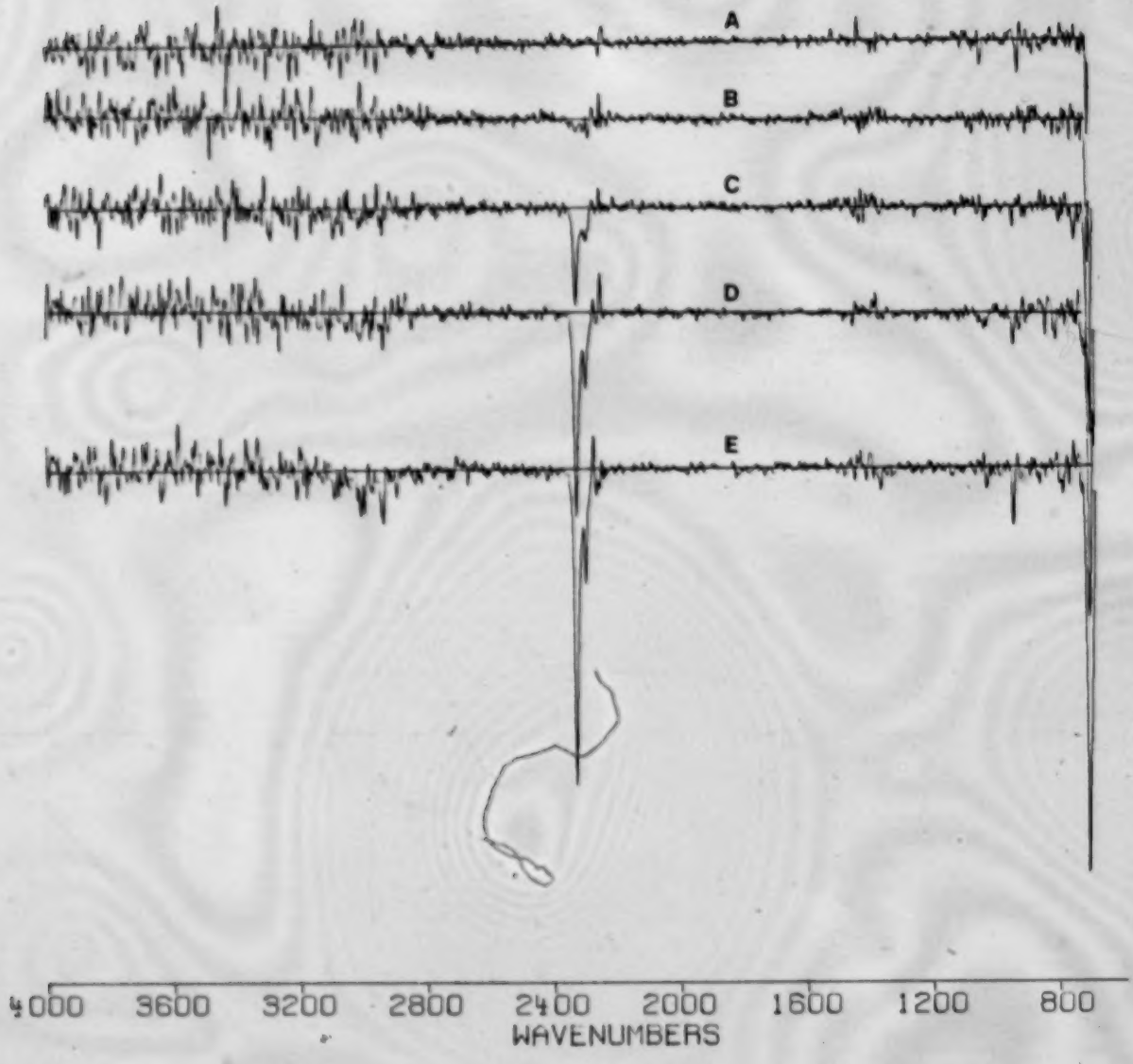

Figure 19. Difference spectra of 0.1 M lithium hexafluoroarsenate in acetonitrile with potential modulation from -0.5V to A. +.5V, B.+1.0V, C.+1.5V D. +2.0V, E. +2.5V.

Table 6

Band positions/cm^{-1} for difference spectra of 0.1 M lithium hexafluoroarsenate in acetonitrile (dry)

Potential step	Pos. displaced bands	Neg. displaced band
-0.5V to +1.0V		708 m
-0.5V to +1.5V		2329 m 2296 w 946 vw 706 s
-0.5V t +2.0V	2274 vw 2253 ww	2940 vw 2329 s 2300 m 947 vw 706 vs
-0.5V to +2.5V	2275 w	3000 vw 2940 w 2329 vs 2301 m 947 m 708 vs

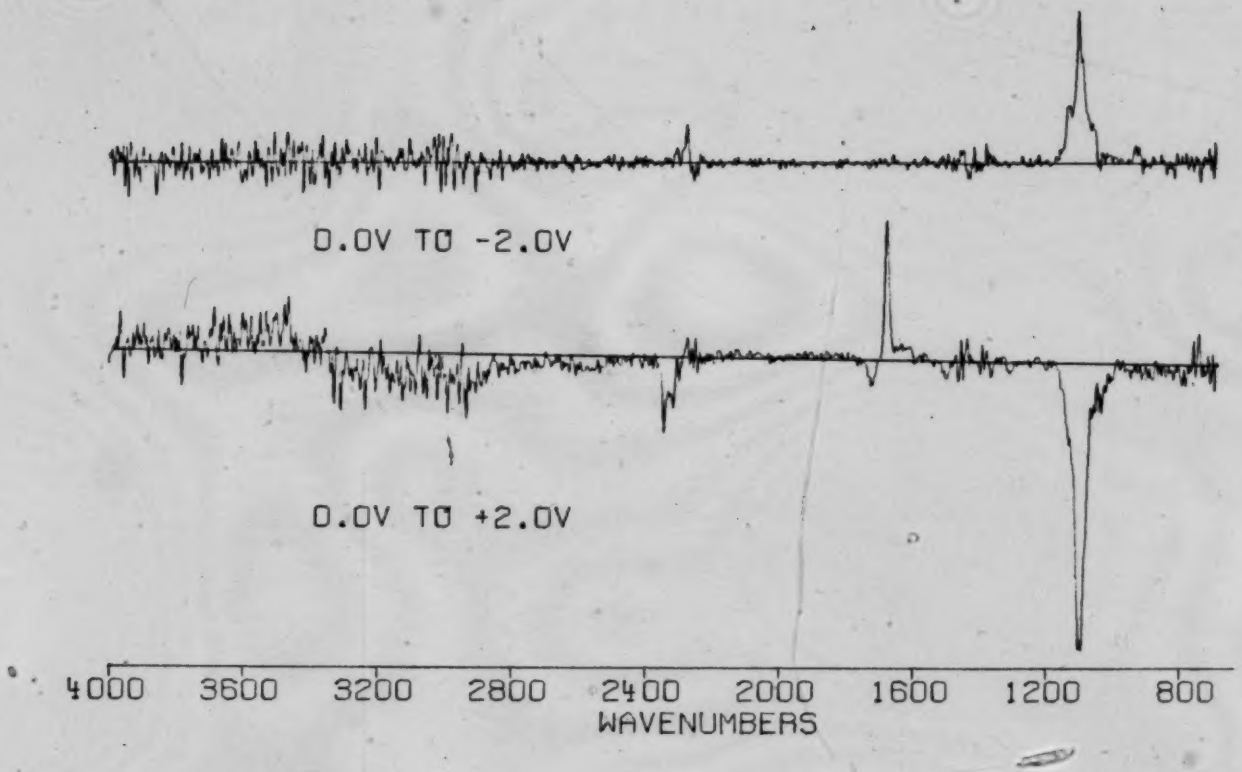

Figure 20. Difference spectra of 0.1M lithium perchlorate in acetonitrile with 0.006% water. Gold mirror electrode.

Table 7

Band positions/cm^{-1} for difference spectra of 0.1 M lithium perchlorate in acetonitrile with 0.006% water (gold electrode)

Potential step	Pos. displaced bands	Neg. displaced band
0.0V to -2.0V	2276 w 1102 s	
0.0V to +2.0V	3540 vw 3380 vw 1678 m	2345 m 2326 w 1724 w 1100 s

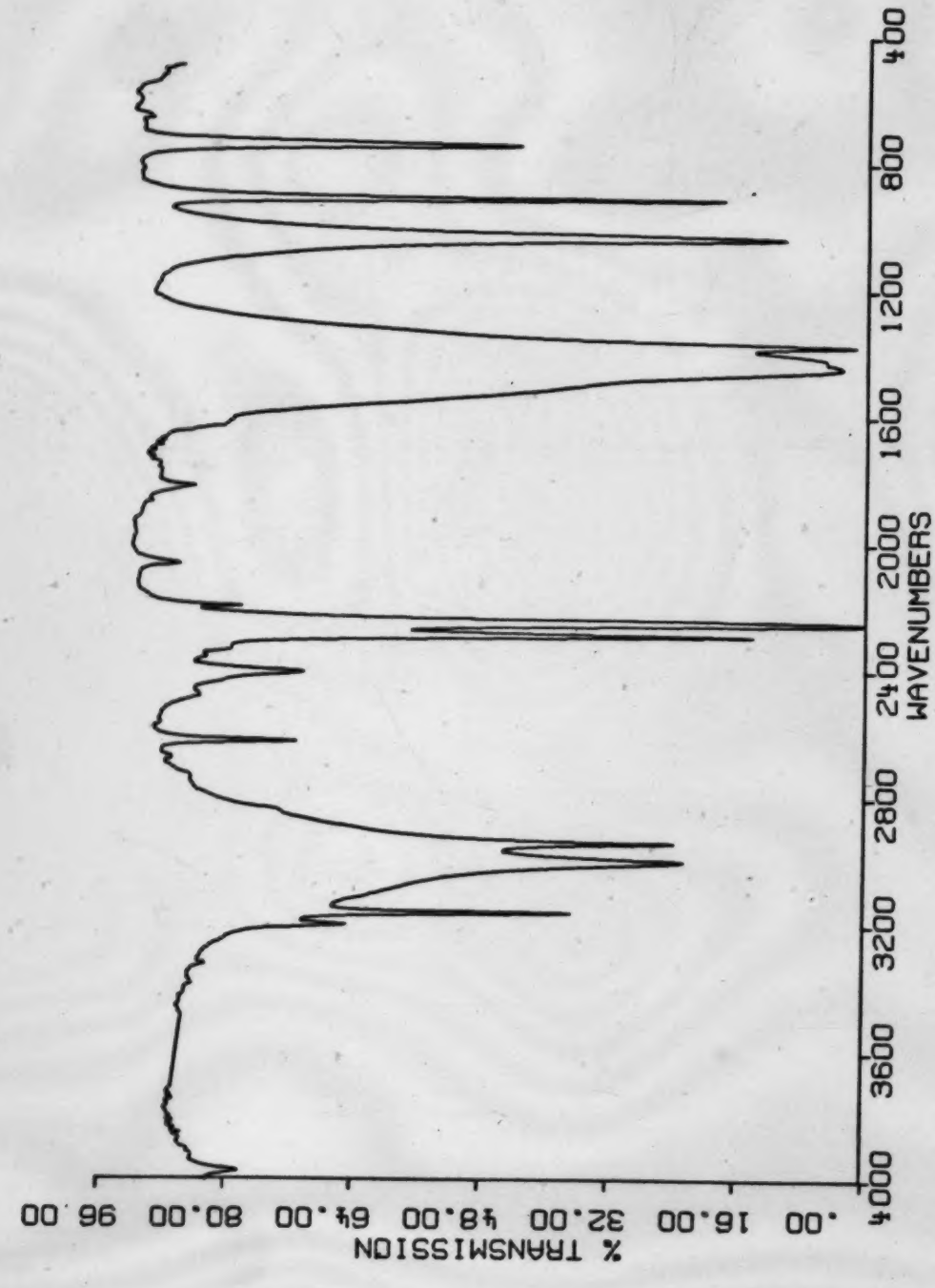

Figure 21. Infrared spectrum of acetonitrile (0.05mm solution cell).

Table 8

Band positions/cm^{-1} for an infrared spectrum of acetonitrile

Observed	Literature (105)[a]	Assignment
3202 w	3203	$2\bar{\nu}_4+\bar{\nu}_3$ (A_1)
3165 m	3165	$\bar{\nu}_2+\bar{\nu}_4$ (A_1)
3001 m	3002	$\bar{\nu}_5$ (e) antisym C-H stretch
2943 m	2944	$\bar{\nu}_1$ (a_1) sym. C-H stretch
2626 w	2628	$\bar{\nu}_2+\bar{\nu}_8$ (E)
2408 w	2411	$\bar{\nu}_3+\bar{\nu}_7$ (E)
2293 s	2293	$\bar{\nu}_3+\bar{\nu}_4$ (A_1)
2254 vs	2254	$\bar{\nu}_2$ (a_1) sym. C N stretch
1443 s	1443	$\bar{\nu}_6$ (e) antisym, CH_3 deformation
1375 vs	1376	$\bar{\nu}_3$ (a_1) sym. CH_3 deformation
1039 s	1047	$\bar{\nu}_7$ (e) antisym. CH_3 rock
918 s	917	$\bar{\nu}_4$ (a_1) sym. C-C stretch

a - values are corrected to vacuum

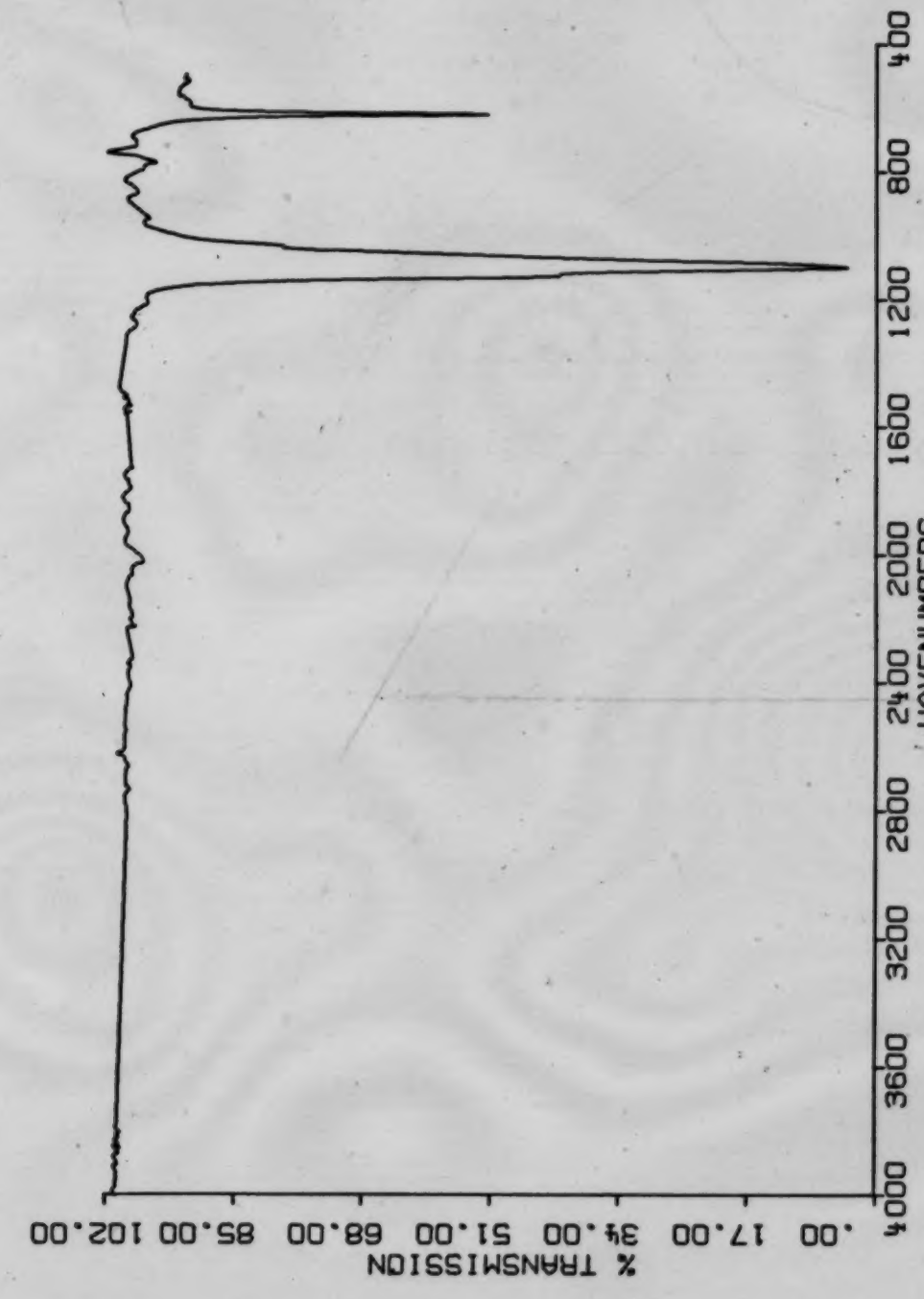

Figure 22. Infrared spectrum of 0.1M lithium perchlorate in acetonitrile(solvent bands subtracted from spectrum).

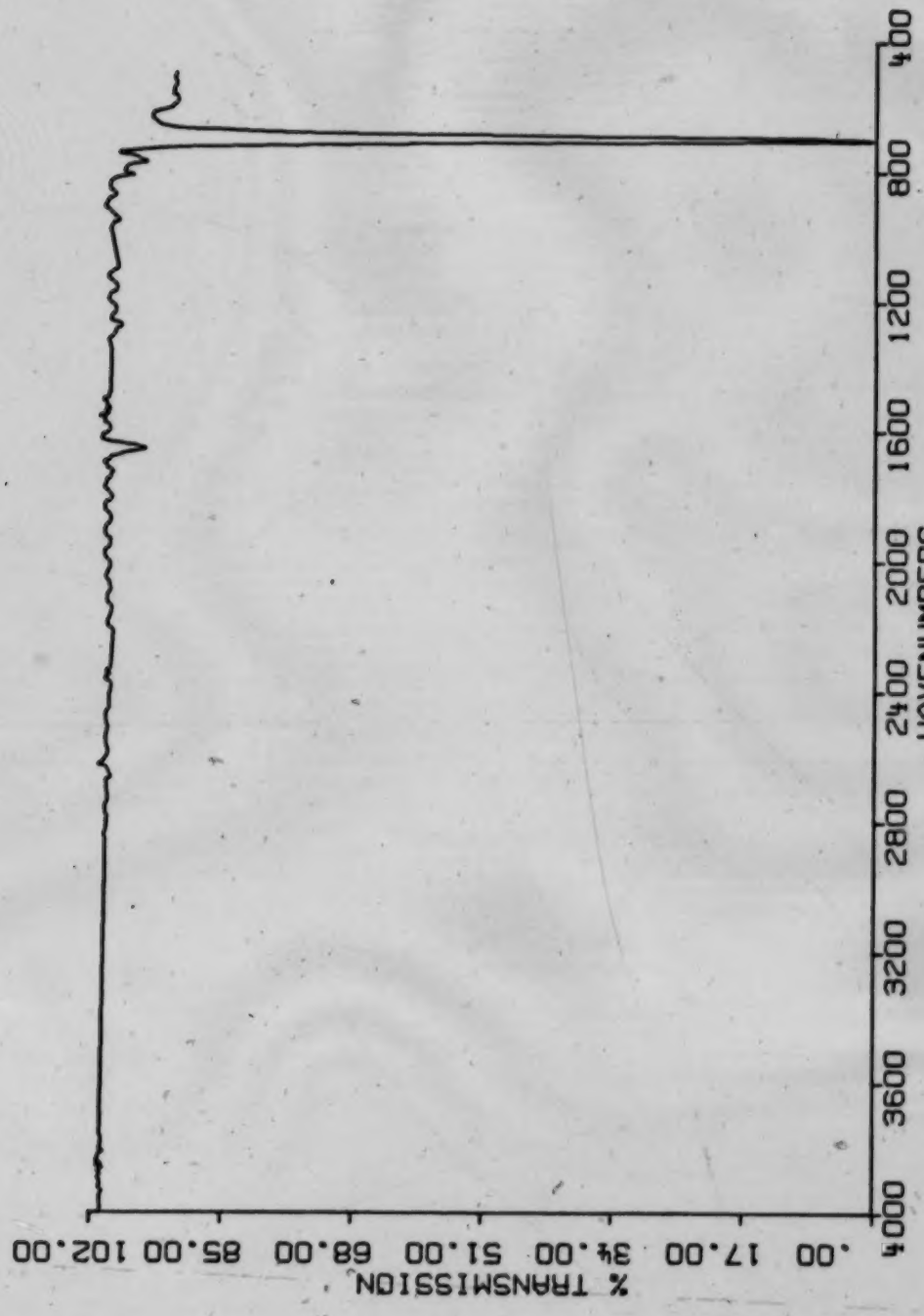

Figure 23. Infrared spectrum of 0.1M lithium hexafluoroarsenate in acetonitrile(solvent bands subtracted from the spectrum).

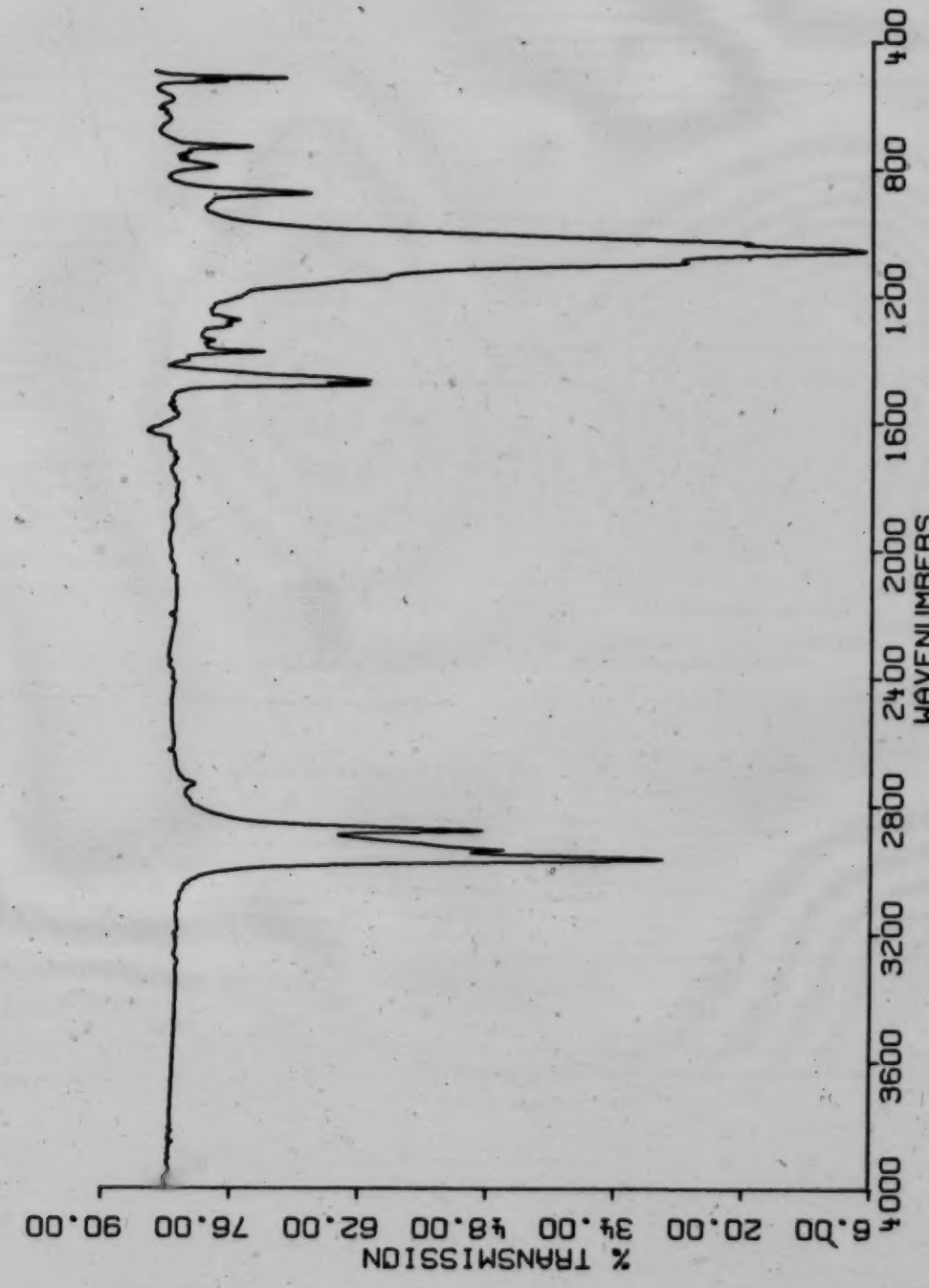

Figure 24. Infrared Spectrum of 0.1 M tetrabutylammonium tetraflororboratein acetonitrile after subtraction of the acetonitrile absorption bands.

Table 9

Infrared Band positions/cm^{-1} for spectra of 0.1M electrolytes in acetonitrile

Electrolyte	Anion	Cation
Lithium perchlorate	ClO_4^- 1102 vs 625 m	Li^+ (no bands in region)
Tetrabutyl ammonium-tetrafluorogorate	BF_4^- 1098 s 1062 vs 1037 s 522 w	Bu_4N^+ 2970 s 2942 m 2881 m 1472 m 1383 w 883 m 739 w
Lithium hexafluoro-arsenate	BF_6^- 706 vs	Li^+ (no bands in region)

difference spectra of this thin layer contain a considerable number of complex absorption bands and their interpretation will give valuable information on the changes in the interphase. First, the absorption bands will be assigned and then an explanation of the potential dependency of the bands will be given.

The difference infrared spectrum of 0.1M tetrabutylammonium tetrafluoroborate in anhydrous acetonitrile or with 0.1M water added has an absorption band 1064 $\pm$ 1 cm^{-1}. The frequency of this band does not change with potential or with the addition of water. The infrared spectrum of 0.1M tetrabutylammonium tetrafluoroborate in acetonitrile is shown in Figure 24. The spectrum has a band at 1062 cm^{-1} which corresponds to the fundamental vibration V_3 (F_2) which is the asymmetric stretch mode of the tetrahedral molecule BF_4^- (107). The infrared spectrum also has two shoulders on the V_3 band which are at 1098 cm^{-1} and 1036 cm^{-1}. These shoulders on the triply degenerate V_3 vibration are due to the loss of Td symmetry of the BF_4^- molecule. The shoulders are also present on the 1064 cm^{-1} band in the difference spectra (Note at 1100 $\pm$ 1 cm^{-1} and 1037 $\pm$ 2 cm^{-1}). Therefore, I conclude that the band at 1064 cm^{-1} in the difference spectra is from the anion (BF_4^-) of the electrolyte.

The difference spectrum of 0.1M lithium perchlorate in anhydrous acetonitrile or with 0.1 M water added, has an absorption band at 1101 $\pm$ 1 cm^{-1}. This absorption band frequency is potential and water concentration independent. The infrared spectrum of the 0.1M lithium perchlorate in acetonitrile has an absorption band at 1102 cm^{-1}.

This band is the asymmetric stretch $\overline{\nu_3}$ (F_2) fundamental vibration of the tetrahedral molecule ClO_4^- (108). Therefore I conclude that the band at 1102 cm^{-1} in the difference spectra is due to the anion (ClO_4^-) of the electrolyte.

The difference spectra of 0.1M lithium hexafluoroarsenate in anhydrous acetonitrile has an absorption band at 707 cm^{-1}. The infrared spectrum of 0.1M lithium hexafluoroarsenate has an absorption band at 706 cm^{-1} which is due to the anion AsF_6^-. Therefore I conclude that the band at 707 cm^{-1} is from the anion (AsF_6^-) of the electrolyte. All of the difference spectra have one band associated with the anion of the electrolyte which is usually the strongest band in the spectra. The reason for this will be explained later.

The tetrabutylammonium tetrafluoroborate electrolyte has the tetrabutylammonium cation, which has infrared vibrations in the spectral region of interest. The difference spectra of 0.1 M tetrabutylammonium tetrafluoroborate in anhydrous acetonitrile or with 0.1M water added, have absorption bands at 2968 $\pm$ 3 cm^{-1}, 2882 $\pm$ 2 cm^{-1} and 1478 $\pm$ 6 cm^{-1}. These bands correspond to absorption bands in the infrared spectrum of 0.1 M tetrabutylammonium tetrafluoroborate in acetonitrile. The tetrabutylammonium cation has vibrations at 2970 cm^{-1}, 2942 cm^{-1}, 2881 cm^{-1}, 1472 cm^{-1}, 1383 cm^{-1}, 883 cm^{-1}, and 739 cm^{-1}. The correlation between the bands in the two types of spectra is close enough to indicate that the potential has little effect on the vibration frequencies of the cation. The bands at 1383 cm^{-1}, 883 cm^{-1} and 739 cm^{-1} are sufficiently weak to be buried in the noise of the difference spectra,

except the band at 2943 cm^{-1} which should be intense enough to be observed but is not. This is due to the fact that acetonitrile has a band in the difference spectra at 2944 cm^{-1} which happens to be displaced in the opposite direction. The origin of this 2944 cm^{-1} band will be explained later. We observe that this acetonitrile band is much more intense than the cation band, and as a result of the digital subtraction process, the cation absorption is masked.

The above assignments of bands in the difference spectra give some insight into the processes occurring in the electrode interphase. When the potential is stepped positive of the pzc the anion is attracted to the electrode to balance the charge. The cation is repelled from the electrode and moves out of the layer. As the potential is stepped more positive of the pzc more of the anion moves into the layer and more of the cation moves out. Now if the potential is stepped negative of the pzc the cation is attracted to the electrode and moves into the layer to balance the charge and the anion is repelled out of the layer. The vibrational frequencies of the cation and the anion are not shifted in wavenumber when comparing these difference spectra of the potential step experiments to the transmission spectrum of the ions in solution. This gives an indication that the ions moving into the thin layer are not adsorbed on the electrode surface. This is not to say that there are not ions adsorbed on the surface, just that there is not an appreciable change in the amount of ions adsorbed on the electrode upon stepping the potential. When a molecule is adsorbed on a metal surface there is a shift in the vibrational frequencies of that molecule due to dipole interactions with the surface.

The difference spectra of the potential step experiment, performed in anhydrous acetonitrile on platinum (Figures 15-20), show five negative displaced bands. The band frequencies are at 3006 ± 5, 2940 ± 2, 2329 ± 1, 2300 ± 2, and 948 ± 2 wavenumbers. The bands are not observed until the potential is stepped to 1.5 volts positive of the pzc and the intensity of the bands increases as the potential is stepped to more positive values. These bands are due to acetonitrile adsorbed on the electrode surface. In the C ≡ N stretching region there are two bands: one at 2329 cm $^{-1}$ and the other at 2300 cm $^{-1}$. According to Irish *et al* (109), when acetonitrile is complexed in solution with metal ions the C ≡ N stretch appears as a doublet. Evans *et al* (110) gave an explanation for this doublet which I used to assign the experimental bands observed herein. Thus the band at 2329 cm $^{-1}$ is assigned to the symmetric C ≡ N stretch $\overline{\nu_2}(s)$ (s-subscript is for adsorbed molecules) and the band at 2300 cm^{-1} is probably a Fermi resonance of $\overline{\nu_2}(s)$ with $\overline{\nu_3}(s) + \overline{\nu_4}(s)$. The band at 948 cm^{-1} is assigned to the symmetric C-C stretch $\overline{\nu_4}(s)$. The bands at 3006 cm^{-1} and 2940 cm $^{-1}$ are assigned to the CH_3 antisymmetric stretch $\overline{\nu_5}(s)$ and the CH_3 symmetric stretch $\overline{\nu_1}(s)$ respectively. The reason that normally infrared active bands of acetonitrile are not observed for the adsorbed acetonitrile is not understood. One reason might be that the vibrations do not follow the surface selection rules.

The $\overline{\nu_2}(s)$ and $\overline{\nu_4}(s)$ bands are shifted 75 cm^{-1} and 30 cm^{-1} respectively to higher frequencies upon adsorption of acetonitrile. The bands $\overline{\nu_1}(s)$ and $\overline{\nu_5}(s)$ are not shifted to any

observable extent. The explanation of the blue shifting of the C ≡ N bond is consistent with the fact the acetonitrile behaves as a Lewis base. This shifting has been reported to occur when acetonitrile forms 1:1 adducts with Lewis acids. Such complex formation leads to a slight decrease in the strength of the π -bonding system and an increase in the strength of the σ-bond between the C and N (111) which increases the C ≡ N force constant.

A gold electrode was substituted for a platinum electrode and the potential step experiment repeated. The $\bar{V}_2(s)$ band at 2346 cm^{-1} on gold is shifted 17 cm^{-1} from that on platinum. This fact indicates that acetonitrile is mostly likely adsorbed on the electrode surface. In addition, Petrii (106) has shown that acetonitrile is strongly adsorbed on the electrode surface and the concentration of acetonitrile adsorbed on the electrode is constant between -1.0V to +1.0V vs Ag/Ag+ reference. This observation correlates well with the difference spectral data, since there is little change in intensity of the bands observed for acetonitrile adsorbed on the electrode until the potential is stepped to 1.5V vs Ag/Ag+ reference. At potential steps more positive, the difference spectra show a decrease in the absorbance of the bulk acetonitrile $\bar{V}_2$ band and an increase in absorbance of the $\bar{V}_2(s)$ band of adsorbed acetonitrile. Thus when the electrode potential is stepped to 2.0 volts greater than pzc, more acetonitrile molecules from the thin layer of solution between the electrode and the window are adsorbed on the electrode surface.

The difference spectra show a decrease in the intensity of the $\bar{\nu}_2$ band of bulk acetonitrile. A very small decrease of $\bar{\nu}_2$ is observed and a large increase in the $\bar{\nu}_2(s)$ is observed. In addition the $\bar{\nu}_2(s)$ band in the difference spectra is much stronger in intensity than all the other bands in the spectrum. A possible explanation for these observations is that acetonitrile is bonded through the nitrogen to the platinum surface, and since the symmetric C $\equiv$ N stretch is blue shifted 75 cm^{-1} upon adsorption, there is a possibility that a charge transfer complex is formed between the C $\equiv$ N and the electrode. The charge transfer complex may give rise to an order of magnitude increase in the intensity of the $\bar{\nu}_2(s)$ band (112).

Water was added to the system and the potential step experiment was duplicated. New bands observed in the difference spectra were at 3632 $\pm$ 10, 3549 $\pm$ 10, 3325 $\pm$ 16, 1691 $\pm$ 20, 1633 $\pm$ 10, and 2265 $\pm$ 2 wavenumbers. If the electrode potential was stepped to values positive of the pzc the bands at 3632 cm^{-1}, 3549 cm^{-1} and 1633 cm^{-1} are positive displaced bands and the bands at 3325 cm^{-1}, 2265 cm^{-1} and 1633 cm^{-1} are negative displaced bands. If the electrode potential was stepped to value negative of the pzc the displacement of the bands reversed. The bands in the O-H stretching region at 3632 cm^{-1} and 3591 cm^{-1} correspond to value reported by Barrow et al (113) of 3640 cm^{-1} and 3545 cm^{-1} for the antisymmetric O-H stretch and the symmetric O-H stretch respectively for a $(MeCN)_2 H_2O$ complex. The band at 2265 cm^{-1} is assumed to be caused by an aceto-nitrile-water interaction (109). The band at 1633 cm^{-1}

is assigned the OH bending of the water in the complex. A possible explanation of the difference spectra is afforded when considering that in solution the $(MeCN)_2 H_2O$ complex is formed throughout the bulk of the solution. When the electrode potential was stepped into a region where acetonitrile is more greatly adsorbed from solution, the acetonitrile from the bulk of solution brings the water complexed with it to the electrode surface. Since the acetonitrile is so strongly absorbed the water probably is not adsorbed on the surface, but it is complexed with acetonitrile on the surface and is in a strongly hydrogen bonded form.

3.3 Conclusion

It is clear from the data presented here that the method employed will be of great value in probing changes in the structure of the electrical double layer.

4.0 Solution Free Measurements

4.1 Results

The infrared difference spectra of the "solution free species" contain spectral features of the neutral and the electrogenerated species. If an absorption band does not change upon the electroactive molecule accepting (or delivering) an electron(s) from (or to) the working electrode, it will not be observed in the difference spectrum. The absorption bands extending above the zero baseline correspond to a decrease in absorbance (or disappearance) of the neutral species. The absorbtion bands extending below the zero baseline correspond to an increase in absorbance (or the formation) of electrogenerated species.

The infrared difference spectrum of 0.01M benzophenone in acetonitrile with 0.1M tetrabutylammonium tetrafluoroborate as the supporting electrolyte, is shown in Figure 25. Table 10 lists the absorption band frequencies. The electrode potential was stepped from -1.75 volts to -2.5 volts vs Ag/Ag^{+} reference electrode. The base and the step potentials were determined from the cyclic voltammogram of the above solution shown in Figure 26, using a previously stated method. The infrared spectrum of 0.2M benzophenone in acetonitrile is shown in Figure 27 (acetonitrile is subtracted from the spectrum). The absorption band frequencies with their vibrational assignments are listed in Table 11.

The infrared difference spectrum of 0.005M anthracene in acetonitrile, with 0.1M tetrabutylammonium tetrafluoroborate as the supporting electrolyte, is shown in Figure 28. Table 12 lists the absorption

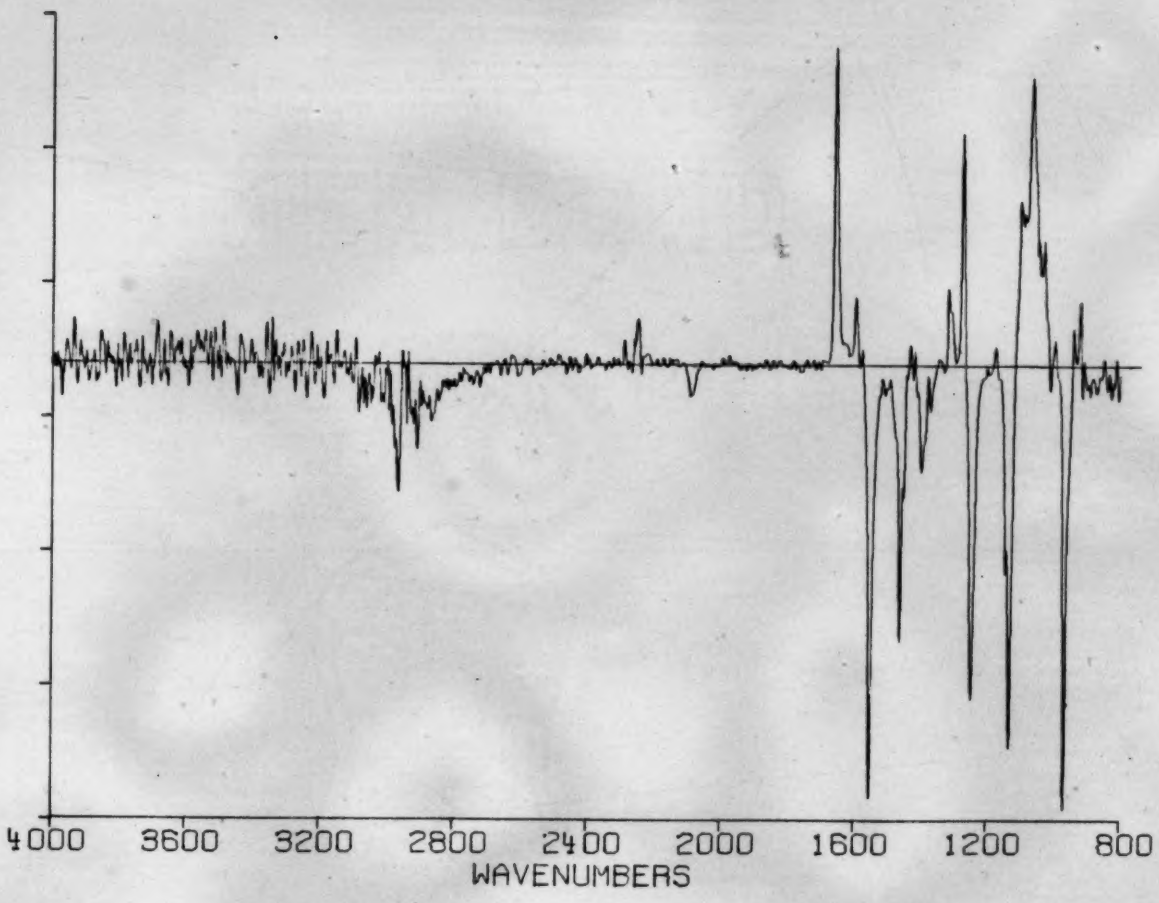

Figure 25. Infrared difference spectrum of 0.01M benzophenone in acetonitrile containing 0.1 M tetrabutylammonium tetrafluoroborate. Electrode modulated from -1.75V to - 2.50 V.

Table 10

Band positions/cm^{-1} for difference spectrum of 0.01M benzophenone in acetonitrile with 0.1M TBAF and pulsed from -1.75 V to -2.5 V vs Ag/Ag^{+}

Positive displaced bands	Negative displaced bands
1661 s	2966 m
1600 m	2942 w
1579 w	2920 w
1319 m	2887 w
1278 s	2193 w
1178 w	1555 s
1095 m	1464 s
1068 s	1401 m
1033 m	1371 w
999 w	1249 s
943 w	1150 sh
922 w	1136 s
	1015 vw
	970 s

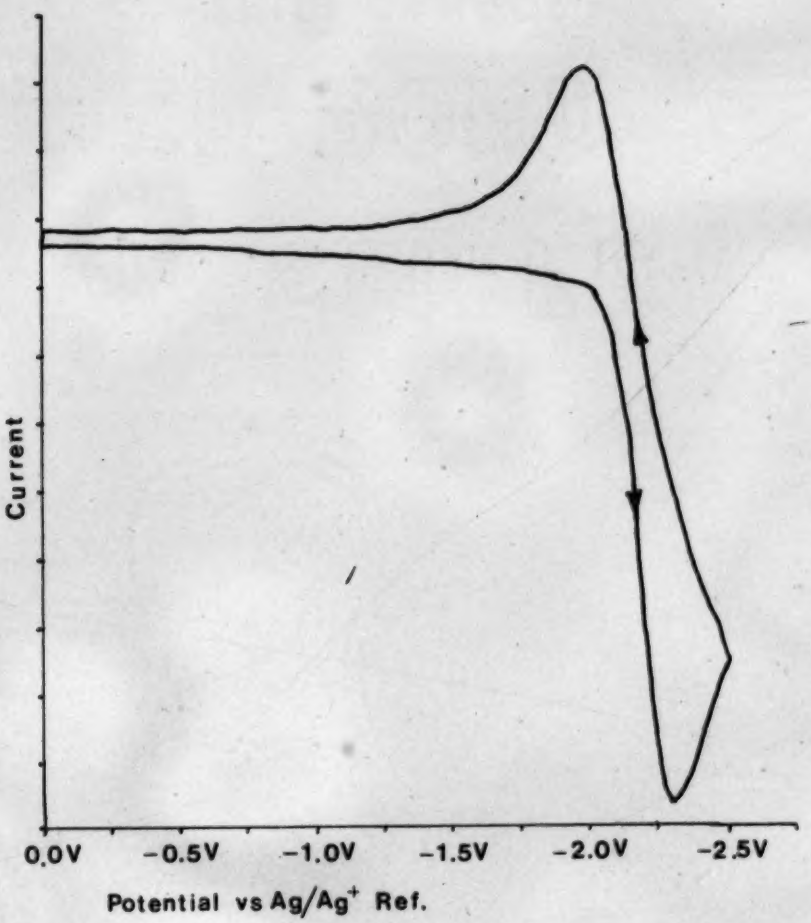

Figure 26. Cyclic voltammogram of 0.01M benzophenone in acetonitrile with 0.1M tetrabutylammonium tetrafluoroborate.

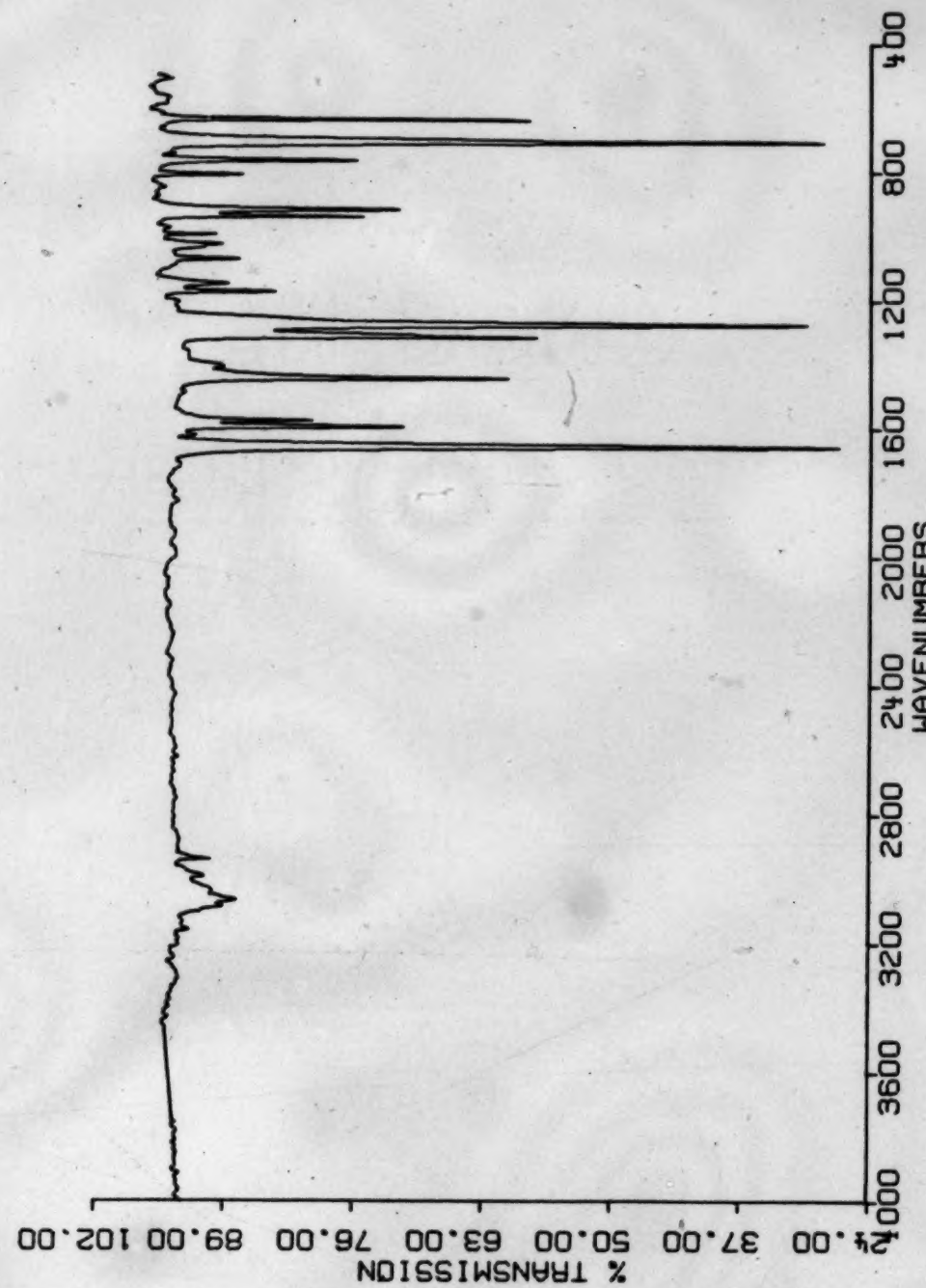

Figure 27. Infrared spectrum of 0.2M benzophenone in actonitrile(solvent bands subtracted from spectrum.)

Table 11

Infrared Band position/cm^{-1} for an infrared spectrum of 0.2 M benzophenone in acetonitrile

Observed	Literature (125)	Assignment (126,90)
3086 vw	3086	
3068 w	3066	
	3061	C-H Stretching
3038 vw	3036	
	3029	
1661 vs	1666	C=O Stretching
1600 m	1601	
1580 w	1580	
1449 s	1448	C-C Stretching
1320 s	1317	
	1306	
1278 vs	1277	
1178 w	1176	
	1158	C-H in Plane Bending
1151 w	1151	
1076 w	1074	
1029 w	1028	
1000 w	1000	Overtone 641+370
	988	
	971	C-H out of Plane Bending
944 m	941	
921 m	917	
	875	
813 w	808	
768 m	760	C-H out of Plane Bending
	718	
709 vs	700	Ring Breathing
640 s	641	C=O Bending

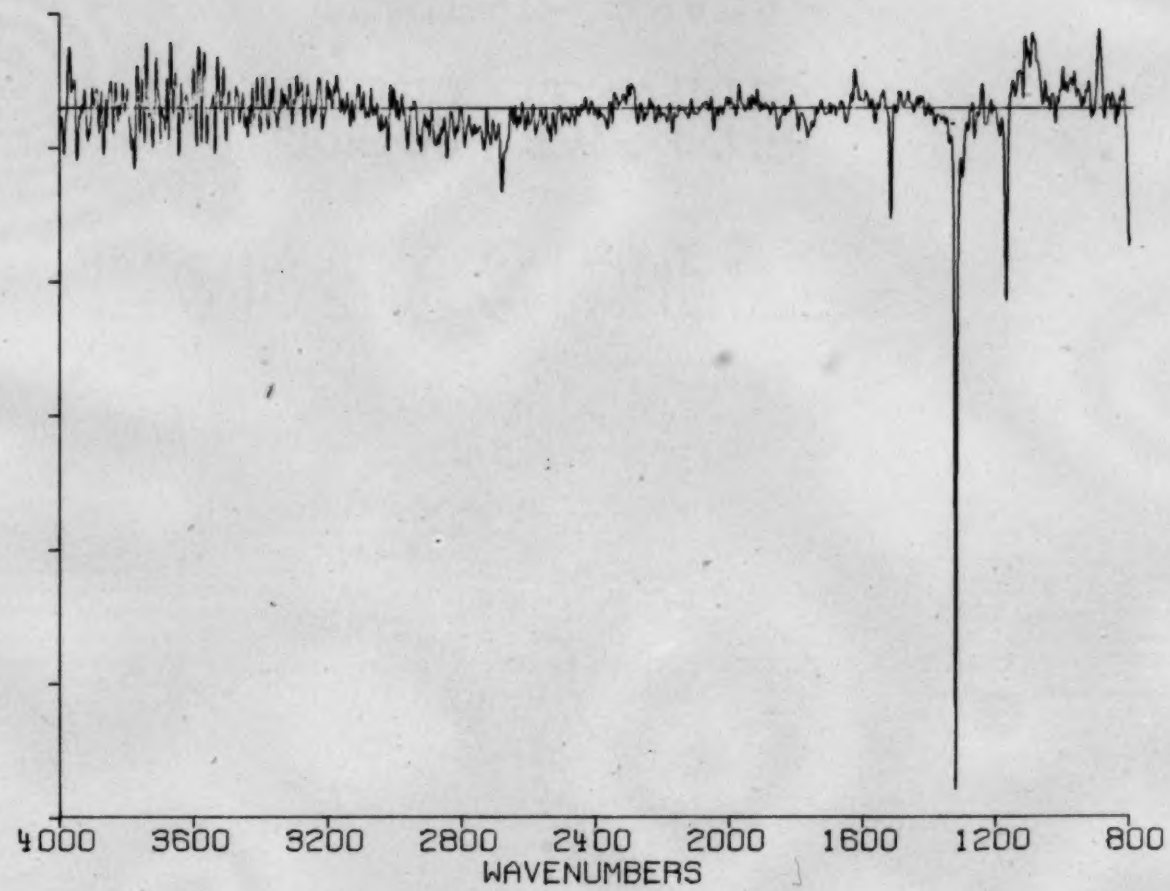

Figure 28. Infrared difference spectrum of 0.005M anthracene in acetonitrile containing 0.1M tetrabutylammonium tetrafluoroborate. Potential modulation -1.5V to -2.5V.

Table 12

Band positions/cm^{-1} for difference spectrum of 0.005 M anthracene in acetonitrile with 0.1 M TBAF and pulsed from -1.5 V to -2.5 V vs Ag/Ag^{+} reference

Positive displaced bands	Negative displaced bands
1623 w	3041 w
1124 vw	2680 vw
1102 w	1516 m
1000 vw	1323 vs
964 vw	1171 m
889 w	

band frequencies. The base and the step potentials were -1.5 volts and -2.5 volts vs Ag/Ag^+ reference electrode respectively. These potentials were determined from the cyclic voltammogram of the above anthracene solution, which is shown in Figure 29. The infrared spectrum of anthracene (KBr disc) is shown in Figure 30. The absorption band frequencies with their assignments are listed in Table 13.

The infrared difference spectrum of 0.005M tetracyanoethylene in acetonitrile with 0.1M tetrabutylammonium tetrafluoroborate as the supporting electolyte, is shown in Figure 31. Table 14 lists the absorption band frequencies. Figure 32 is an expansion of Figure 31 to observe the small absorptions. The base and the step potentials were +0.25 volts and -0.25 volts vs Ag/Ag^+ reference electrode respectively. These potentials were determined from the cyclic voltammogram of the above tetracyanoethylene solution, which is shown in Figure 33. The infrared spectrum of tetracyanoethylene (KBr disc.) is shown in Figure 34. The absorption band frequencies with their assignments are listed in Table 15.

Figure 29. Cyclic voltammogram of 0.005 M anthracene in acetonitrile containing 0.1 M tetrabutylammonium tetrabutylammonium tetrafluoroborate.

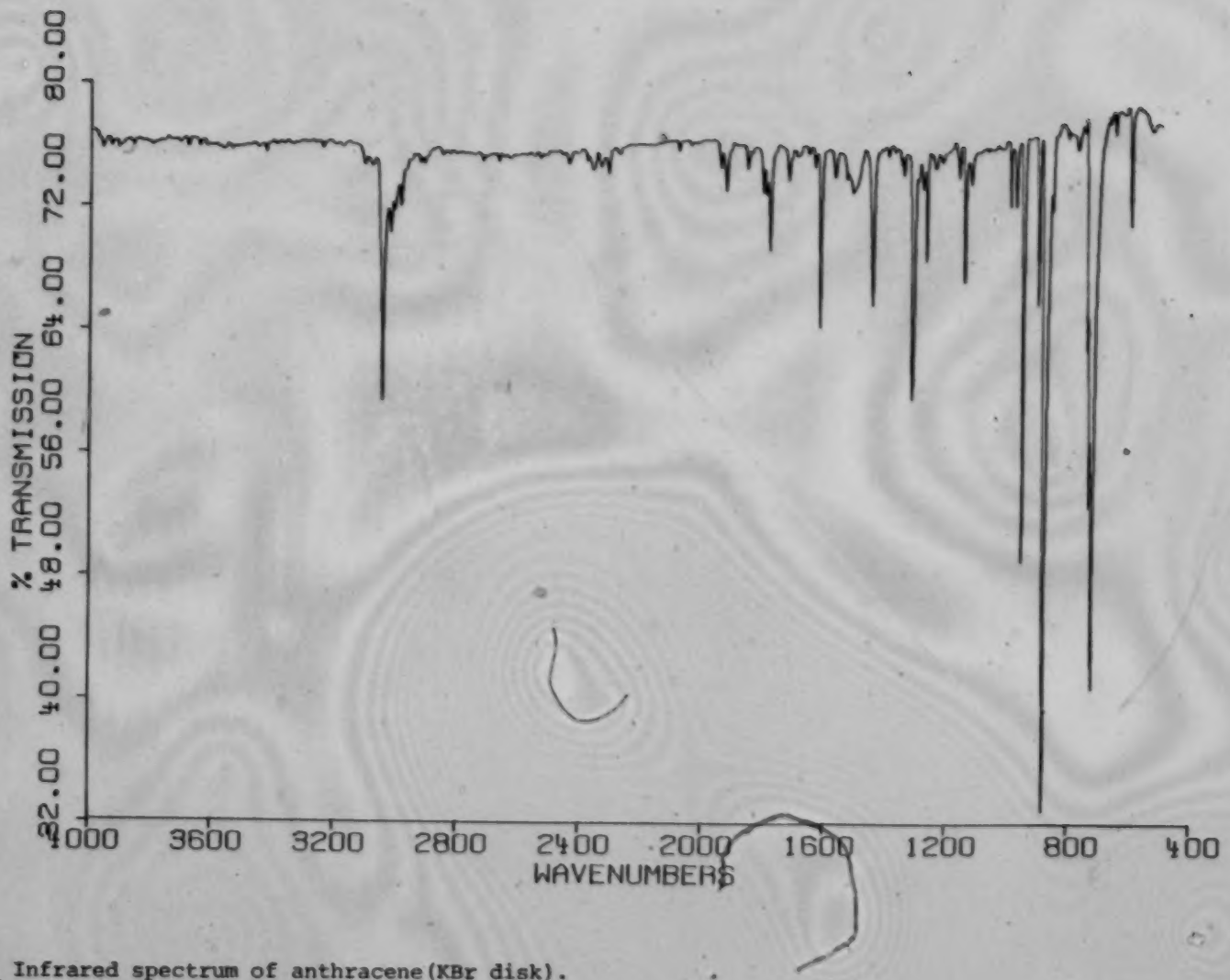

Figure 30. Infrared spectrum of anthracene(KBr disk).

Table 13

Infrared band position/cm^{-1} for an infrared spectrum of Anthracene (KBr Disc.)

Observed	Literature (91)[1]	Assignment (91)
	3089	b_{3u} C-H stetch
3048 m	3058	b_{2u} C-H stretch
3022 w	3026	b_{2u} C-H stretch
	3016	
2987 w		
	2972	b_{2u} C-H stretch
1928 w	1935	
1808 w	1815	
1784 m	1794	
1724 w	1733	
	1705	
	1674	
1620 m	1623	b_{2u} ring stretch
1533 vw	1536	b_{3u} ring stretch
	1462	b_{3u} ring stretch
1448 m	1447	b_{2u} ring stretch
	1398	b_{3u} ring stretch
1347 vw	1344	
1315 m	1316	b_{2u} ring stretch
1272 w	1269	b_{2u} in plane bend
1166 vw	1165	b_{3u} in plane bend
1146 m	1148	b_{2u} in plane bend
1126 vw	1126	
999 w	999	b_{3u} in plane bend
956 s	954	b_{1u} C-H out of plane bending
906 m	906	b_{2u} skeletal deformation
884 vs	883	b_{1u} C-H out of plane bending
860 w		b_{1u} C-H out of plane bending
735 m		b_{1u} C-H out of plane bending
725 s	727	b_{1u} C-H out of plane bending
601 m	600	b_{1u} skeletal deformation

1 - in solution

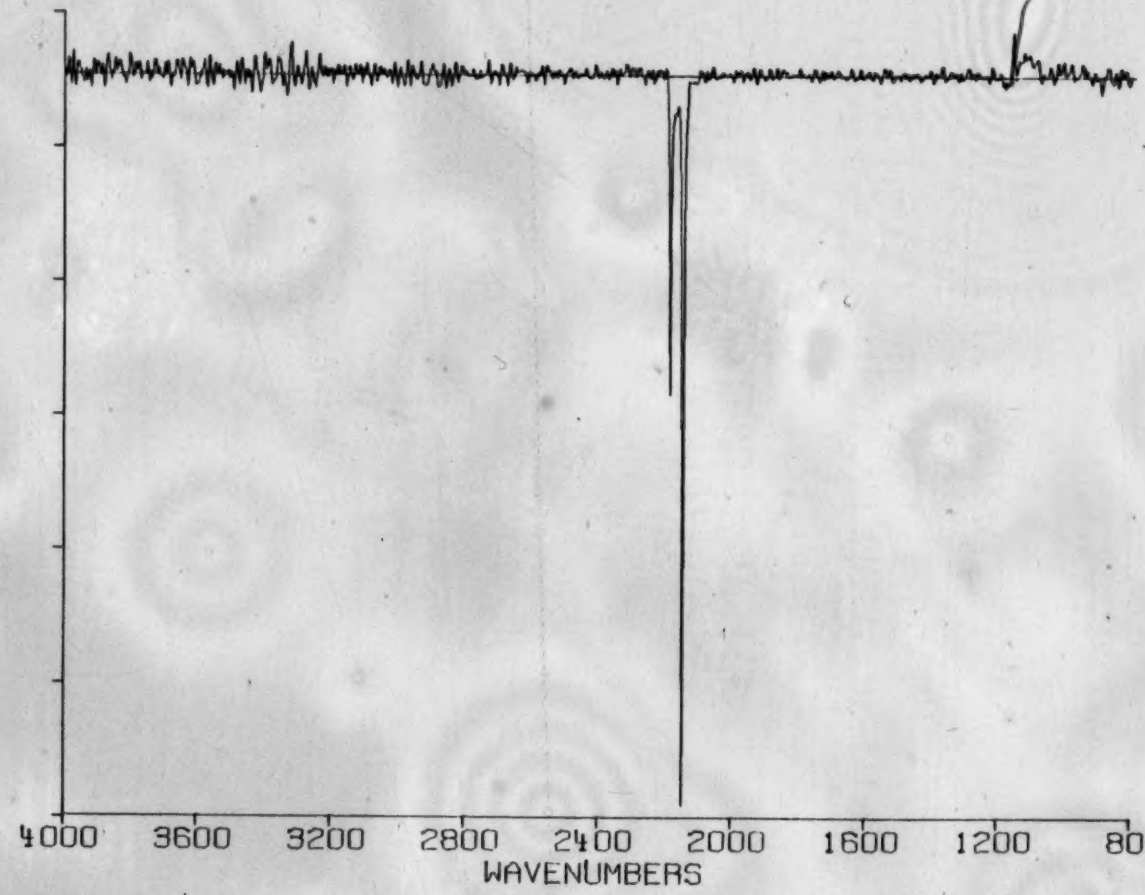

Figure 31. Infrared difference spectrum of 0.005 M tetracyanoethylene in acetonitrile containing 0.1M tetrabutylammonium tetrafluoroborate. Potential modulation from +0.250 to - 0.250 V.

Table 14

Band positions/cm^{-1} for tetracyanoethylene pulsed from +0.25V to -0.25V *vs* Ag/Ag^{+} reference.

Positive displaced bands	Negative displaced bands
1155 w	2187 m
1123 vw	2148 vs
1083 vw	1181 vw
1022 vw	891 w
950 vw	

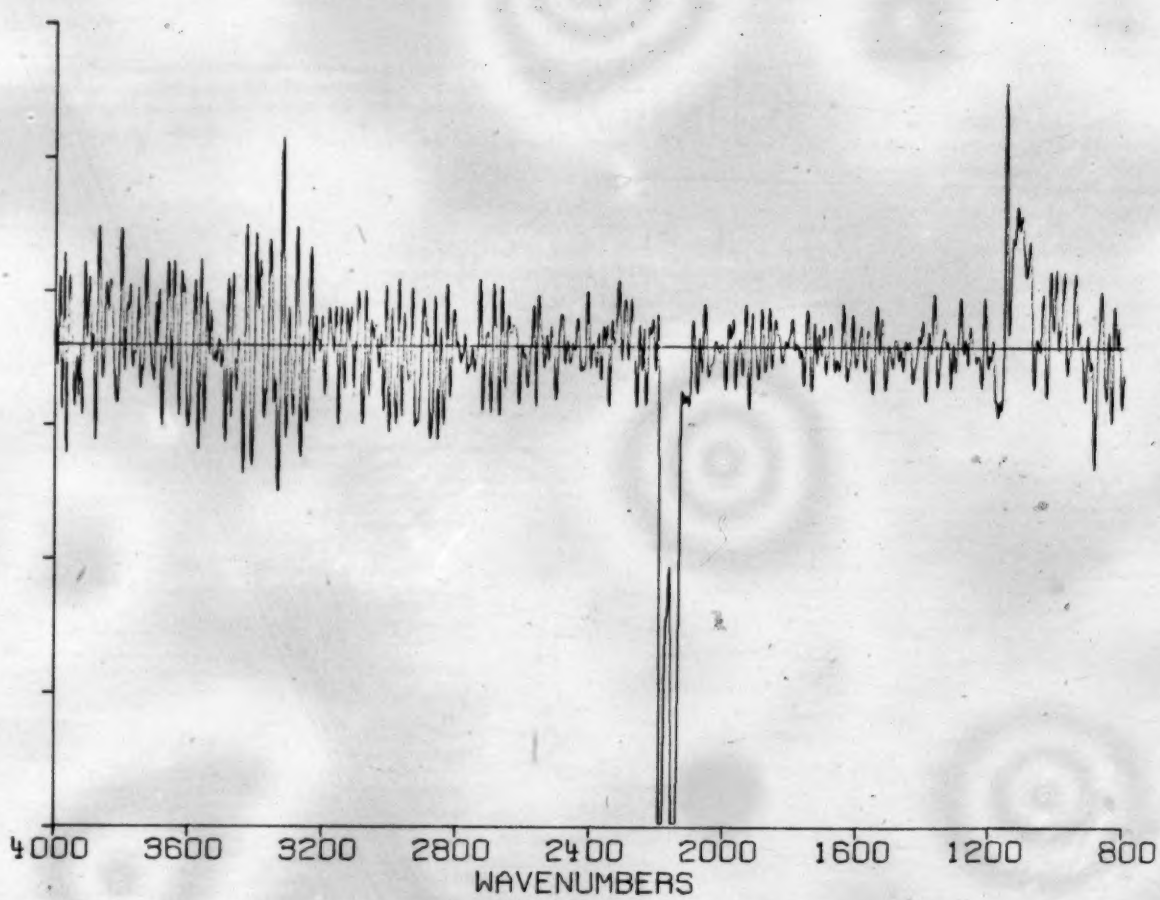

Figure 32. Expansion of figure 31.

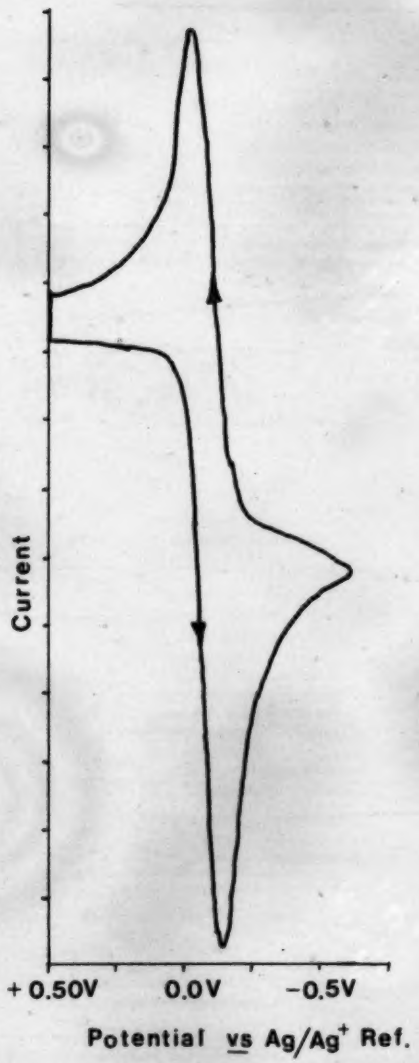

Figure 33. Cyclic voltammogram of 0.005M tetracyano ethylene in acetonitrile containing 0.1M tetrabytylammonium tetrabutylammonium tetrafluoroborate.

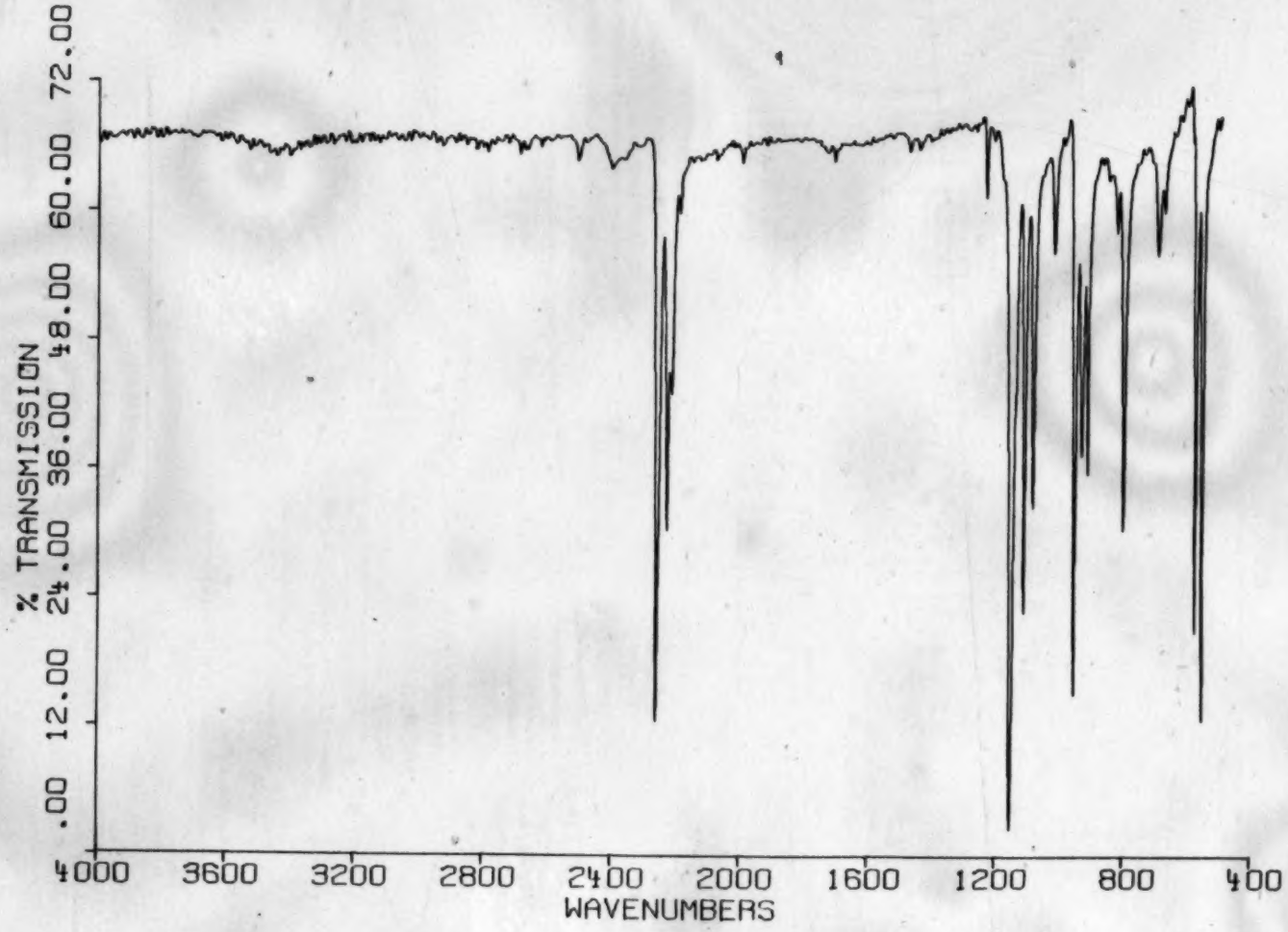

Figure 34. Infrared spectrum of tetracyanoethylene (KBr disk).

Table 15

Infrared band position/cm^{-1} for an infrared spectrum of tetracyanoethylene in KBr disc.

Observed	Literature (124)	Assignment (124)
2262 vs	2262	ν_9 b_{1u} C N stretch
2228 s	2229	ν_{15} b_{2u} C N Stretch
2215 m	2214	
2192 w	2202	
1234 w	1232	
	1209	
1155 vs	1155	ν_{16} b_{2u} C-C Stretch
	1139	
1115 s	1114	
1086 s	1086	
1021 m	1020	
959 vs	959	ν_{16} b_{1u} C-C stretch
934 s	934	
917 s	915	
825 w	823	
803 s	804	
	796	
	715	
697 m	693	
676 w	671	
578 s	579	ν_{11} b_{1u} C-C N bend
556 vs	556	ν_{23} b_{3u} C-C N out of plane bend
	537	
	442	ν_{24} b_{3u} (CN)-C-(CN) out of plane wag
427 m	428	ν_{12} b_{2u} C-C N bend

4.2 Discussion

Three model compounds (tetracyanoethylene, anthracene, and benzophenone) were used to test whether this technique is a viable method for studying electrogenerated molecular ions in solution. The vibrational modes of the anion radicals produced from these compounds have been studied previously by infrared spectroscopy (47, 114-119) and by resonance Raman spectroscopy (56, 120-123). These particular compounds were chosen because of the relative stability of the anion radicals in anhydrous acetonitrile.

The difference spectrum of benzophenone shows changes in the absorption band frequencies from the neutral molecule to the anion radical. From the difference spectrum the C=O stretching frequency shifts from 1661 cm^{-1} in the neutral molecules to 1555 cm^{-1} in the anion radical. This shift is attributed to the fact that since the lowest unoccupied molecular orbital contains a significant contribution from the C =O band, it will be that bond that is most affected by electron transfer (120). This is the orbital that the added electron will most likely occupy. Aleksandrov et al (123) stated that the added electron is localized in the C=O orbital and also indirectly effects the ring vibrations. Both of these effects are apparent in the difference spectrum. The technique used in this study was compared with other techniques (47, 119, 120) for studying the vibrational modes of benzophenone anion radical. Table 16 gives a comparison of the absorption bands determined in each technique. It is seen from the table that the technique used in this study correlated well with the other techniques.

Table 16

Comparison of band positions/cm^{-1} for benzophenone anion radical

Observed	Tallant[1]	Aleksandrov[2]	Juchnovski[3]
2966			
2942			
2920			
2887			
2193			
		1591	
1555	1535-1550	1551	1560
		1480	
1464	1455	1454	
1401	1355-1405	1403	1396
1371			
			1322
			1288
1249	1225-1255		1260
		1183	
1150		1145	1150
1136			1143
		1080	
		1027	
1015			1019
		993	
970			976
			814

1) Ref. 47 IRS in DMSO
2) Ref. 120 in THF (resonance raman)
3) Ref. 119 in THF (infrared)

Table 17

Comparison of band position/cm^{-1} for anthracene anion radical

Observed	Li (116)
3041 w	
2680 vw	
	1564
1516 m	1515
	1448
	1383
1323 vs	1320
1171 m	1173
	1023

A spectrum more difficult to interpret is that of the difference spectrum of anthracene. The absorption bands of the anthracene anion radical appear to be much more intense than the absorption bands of the neutral molecule. The reason for this observation is not understood. The absorption bands observed for the anthracene anion radical correlate well with those determined in a study by Li et al (116) on the potassium salts of anthracene. The bands observed for one potassium salt (one potassium to two anthracene molecules) correlated with the anthracene anion radical generated in this work. (See figure 28 page 89). The absorption frequencies found in Li's work and this one are compared in Table 17.

In the difference spectrum of tetracyanoethylene there are two very intense bands observed at 2148 cm^{-1} and 2187 cm^{-1} for the anion radical. These two bands are assigned to the C≡N stetch, which agree with Devlin et al's (114) assignment. The neutral molecule also has two C≡N stretches $\overline{\nu}_9$ and $\overline{\nu}_{15}$ (124). The decrease in absorbance of the C≡N stretch of the neutral species should be observed but it is not. A possible explanation of this is that the band at 2261 cm^{-1} for tetracyanoethylene is masked by a much more intense band at 2254 cm^{-1} for acetonitrile, thereby preventing a proper subtraction. The change in the C-C stretching frequency is also observed in the difference spectrum. The C-C stretch of the neutral species(ν_{16}) at 1155 cm^{-1} shifts to 1181 and the C-C stretch of the neutral species(ν_{10}) at 950 cm^{-1} shifts to 891 cm^{-1} when the anion radical is formed. The results reported previously by Li and Devlin are complimentary to those reported

in this study. This is because the anion radical is in solution and the stretch is not infrared active. The reason Devlin et al observed this band in the solid state is because of a charge oscillation activation (112) of the C=C symmetric stretch $\overline{\nu}_2$ which is produced in the alkali metal salt of tetracyanoethylene. The tetracyanoethylene anion radical is probably not involved in any charge transfer complex that will give rise to the charge oscillation activation of $\overline{\nu}_2$. Thus the C=C symmetric stretch $\overline{\nu}_2$ is not observed.

4.3 Conclusion

The new technique described is a simple convenient method for obtaining spectra of electrogenerated species. If a molecular ion can be generated electrochemically then it is probable that its infrared spectrum can be obtained by using the described technique. Previously it has been difficult to obtain infrared spectra of molecular ions in solution because of sample handling and the large infrared absorptions of the solvents used when generating molecular ions. In this study, such effects are minimized by the use of extremely thin layers of solution.

This technique sheds new light on the subject of studying molecular ions. When an electron(s) is added or removed from a molecular orbital of a neutral molecule there is usually some change in the molecular structure which in turn may change the symmetry and the bonding of the molecular ion from that of the neutral molecule. This technique provides a unique simple method for observing such changes.

REFERENCES

1. A. Bewick, K. Kunimatsu and B.S. Pons, Electrochim. Acta, 25 (1980) 465.

2. A Bewick, and K. Kunimatsu, Surf. Sci., 101 (1980) 131.

3. A. Bewick, K. Kunimatsu, J. Robinson and J.W. Russell, J. Electroanal. Chem., 119 (1981) 175.

4. T. Davidson, B. Stanley Pons, A. Bewick and P.P. Schmidt, J. Electroanal, Chem., 132 (1982) 329.

5. A. Bewick and J.W. Russell, J. Electroanal, Chem., 132 (1982) 329.

6. B. Benden, A. Bewick, C. Lamy and K. Kunimatsu, J. Electroanal., Chem., 121 (1981) 343.

7. T. Kuwana, R.K. Darlington, and D.W. Leedy, Anal. Chem., 36 (1964) 2023.

8. A. Bewick and A.M. Tuxford, J. Electroanal. Chem., 47 (1973) 255.

9. H.B. Mark and E. Randall, Symp. of the Faraday Soc., 4 (1970) 157.

10. R. Memming and F. Mollers, Symp. of the Faraday Soc., 4 (1970) 145.

11. W. Plieth, Symp. of the Faraday Soc., 4 (1970) 138.

12. D. Laser and M. Ariel, J. Electroanal. Chem., 35 (1972) 405.

13. A. Trifonov and I. Schopov, J. Electroanal. Chem., 35 (1972) 415.

14. A. Bewick and A.M. Tuxford, Symp. of the Faraday Soc., 4 (1970) 114.

15. E. Yeager, Surf. Sci., 101 (1980) 1.

16. M. Fleischman and I.R. Hill in J.O'M. Bockris and B.E. Conway (Eds.), Modern Aspects of Electrochemistry, Plenum Press, New York, in press.

17. T. Kuwana and N. Winograd in A.J. Bard (Ed.), Electroanalytical Chemistry, Vol. 7, Marcel Dekker, New York, 1974, p. 1.

18. T. Kuwana, Ber. Bunsenges. Phys. Chem., 77 (1973) 858.

19. A. Bewick, J.M. Mellor and B.S. Pons, Electrochim. Acta, 25 (1980) 931.

20. T. Kuwana and W.R. Heineman, Acc. Chem. Res., 9 (1976) 241.

21. E.A. Blubaugh, A.M. Yacynych and W.R. Heineman, Anal. Chem., 51 (1979) 561.

22. W.R. Heineman, Anal. Chem., 50 (1978) 390A.

23. V. Strojek and T. Kuwana, J. Electroanal. Chem., 16 (1968) 471.

24. N. Winograd and T. Kuwana, J. Electroanal. Chem., 23 (1969) 333.

25. G. Grant and T. Kuwana, J. Eletroanal. Chem., 24 (1970) 24.

26. N. Wingrad, H. Blount and T. Kuwana, J. Phys. Chem., 73 (1969) 3456.

27. W. von Benken and T. Kuwana, Anal. Chem., 42 (1970) 1114.

28. W. Heineman and T. Kuwana, Anal. Chem., 43 (1971) 1075.

29. W. Heineman and T. Kuwana, Anal. Chem., 44 (1972) 44.

30. J.F. Tyson and T.S. West, Talanta, 26 (1979) 117.

31. J.F. Tyson and T.S. West, Talanta, 27 (1980) 335.

32. C.E. Baumgartner, G.T. Marks, D.A. Alkens, H.H. Richtol, Anal. Chem., 52 (1980) 267.

33. R. Pruiksma, J. Electroanal. Chem., 144 (1980) 147.

34. R.L. McCreery, R. Pruiksma and R. Fagan, Anal. Chem., 51 (1979) 749.

35. A.W.B. Aylmer - Kelly, A. Bewick, P.R. Cantrill and A.M. Tuxford, Discuss. Faraday Soc., 56 (1973) 96.

36. J.D.E. McIntyre in R.H. Muller (Ed.), Advances in Electrochemistry and Electrochemical Engineering, Vol. 9, John Wiley and Sons, New York, 1973, p. 61.

37. J.F. Goeltz and W.R. Heineman, J. Electroanal. Chem, 109 (1979) 155.

38. D. Laser and M.A. Ariel, J. Electroanal. Chem., 41 (1973) 381.

39. W.N. Hansen, T. Kuwana and R.A. Osteryoung, Anal. Chem., 38 (1966) 1810.

40. V.S. Srinivasan and T. Kuwana, J. Phys. Chem., 72 (1968) 1144.

41. A. Prostak, H.B. Mark and W.N. Hansen, J. Phys. Chem., 72 (1968) 2576.

42. A.H. Reed and E. Yeager, Electrochim. Acta, 15 (1970) 1345.

43. H.B. Mark and B.S. Pons, Anal. Chem., 38 (1966) 119.

44. B.S. Pons, J. Manson, L. Winstron and H.B. Mark, Anal. Chem., 39 (1967) 685.

45. J.F. Goelz, A.M. Yacynych, H.B. Mark and W.R. Heineman, J. Electroanal. Chem., 103 (1979) 277.

46. W.N. Hansen in R.H. Muller (Ed.), Advances in Electrochemistry and Electrochemical Engineering, Vol. 9, John Wiley and Sons, New York, 1973, p. 1.

47. D.E. Tallant and D.H. Evans, Anal. Chem., 41 (1969) 835.

48. N.J. Harrick, Internal Reflection Spectroscopy, John Wiley and Sons, New York, 1967.

49. B.D. Cahan and R.F. Spanier, Surf. Sci., 16 (1969) 166.

50. B.D. Cahan, Surf. Sci., 56 (1976) 354.

51. R.H. Muller in R.H. Muller (Ed.), Advances in Electrochemistry and Electrochemical Engineering, Vol. 9, John Wiley and Sons, New York, 1973, p. 167.

52. J. Kruger in R.H. Muller (Ed.), Advances in Electrochemistry and Electrochemical Engineering, Vol. 9, John Wiley and Sons, New York, 1973, p. 227.

53. W.R. Heineman, M.L. Meckstroth, B.J. Norris and C. Su, J. Electroanal. Chem., 104 (1979) 577.

54. M. Petek, T. Neal and R. Murray, Anal. Chem., 43 (1971) 1069.

55. J.S. Clarke, A.T. Kuhn and W.J. Orville- Thomas, J. Electroanal. Chem., 54 (1974) 253.

56. D.L. Jeanmaire, M.R. Suchanski and R.P. Van Duyne, J. Am. Chem. Soc., 97 (1975) 1699.

57. M.R. Suchanski and R.P. Van Duyne, J. Am. Chem. Soc., 98 (1976) 250.

58. D.L. Jeanmaire and R.P. Van Duyne, J. Am. Chem. Soc., 98 (1976) 4029.

59. D.L. Jeanmaire and R.P. Van Duyne, J. Am. Chem. Soc., 98 (1976) 4029.

60. D.L. Jeanmaire and R.P. Van Duyne, J. Electroanal Chem., 66 (1975) 235.

61. M. Fleischmann, P.J. Hendra and A.J. McQuillan, J. Chem. Soc. Chem. Commun., (1973) 80.

62. M. Fleischman, P.J. Hendra and A.J. McQuillan, Chem. Phys. Lett., 26 (1974) 163.

63. D.L. Jeanmaire and R.P. Van Duyne, J. Electroanal. Chem., 84 (1977) 1.

64. S.G. Schultz, M. Janick-Czachor and R.P. Van Duyne, Surf. Sci., 104 (1981) 419.

65. T. Maniu and H. Metiu, Surf. Sci., 101 (1980) 399.

66. F.R. Aussenegg and M.E. Lippitsch, Chem. Phys. Lett., 50 (1978) 214.

67. G.C. Schatz and R.P. Van Duyne, Surf. Sci., 101 (1980) 425.

68. S.L. McCall and P.M. Platzman, Phys. Rev. B: Condens. Matter, 22 (1980) 1660.

69. W.H. Weber and G.W. Ford, Phys. Rev. Lett., 44 (1980) 44.

70. J. Gersten and A. Nitzan, J. Chem. Phys., 73 (1980) 3023.

71. A. Regis and J. Corset, Chem. Phys. Lett., 70 (1980) 305.

72. C.D. Jaeger and A.J. Bard, J. Phys. Chem., 67 (1979) 3146.

73. T.M. McKenney in A.J. Bard (Ed.), Electroanalytical Chemistry, Vol. 10, Marcel Dekker, New York, 1979, p. 97.

74. R. Adams, J. Electroanal. Chem., 8 (1964) 151.

75. W.E. O'Grady and J. O'M. Bockris, Surf. Sci, 38 (1973) 249.

76. H. Meirer, V. Tschirwitz, E. Zimmerhackl, W. Albrecht and G. Zeitler, J. Phys. Chem., 81 (1977) 712.

77. A.T. Hubbard, R.M. Ishikawa and J. Kalekaau, J. Electroanal. Chem., 86 (1978) 271.

78. R.N. Ross, J. Electroanal. Chem., 76 (1977) 139.

79. R.N. Ross, J. Electrochem. Soc., 126 (1979) 67.

80. R.M. Ishikawa and A.T. Hubbard, J. Electroanal. Chem., 69 (1976) 317.

81. S.W. Feldberg in A.J. Bard (Ed.), Electroanalytical Chemistry, Vol. 3, Marcel Dekker, New York, 1969, p. 199.

82. L.F. Whiting and P.W. Carr, J. Electroanal. Chem., 81 (1977) 1.

83. B.S. Pons and P.P. Schmidt, Electrochim, Acta, 25 (1980) 987.

84. B.S. Pons, T. Davidson and A. Bewick, in preparation.

85. B.S. Pons, T. Davidson and A. Bewick, in preparation.

86. B.S. Pons, T. Davidson and A. Bewick, in preparation.

87. W.J. Anderson and W.N. Hansen, J. Electroanal. Chem., 47 (1973) 229.

88. R.G. Greenler, J. Chem. Phys., 44 (1966) 310.

89. R.G. Greenler, J. Chem. Phys., 50 (1969) 1963.

90. K.M. Rao and C.K. Narayanaswamy, Indian, J. of Pure and Applied Phys., 8 (1970) 100.

91. S. Califano, J. Chem. Phys., 36 (1962) 903.

92. C.K. Mann, J. O'Donnell and J. Ayers, Anal. Chem., 37 (1965) 1161.

93. H. Lund and P. Iverson in M. Baizwer (Ed.), Organic Electrochemistry, Marcel Dekker, New York, 1973.

94. Andrzej Lasia, J. Electroanal. Chem., 102 (1979) 117.

95. T.L. Cairns, R.A. Carboni, D.D. Coffman, V.A. Engelhardt, R.E. Heckert, E.L. Little, E.G. McGeer, B.C. McKusick, W.V. Middleton, R.M. Scribner, C.W. Thebald and H.E. Winberg, J. Am. Chem. Soc., 80 (1958) 2775.

96. I.M. Kolthoff and J.E. Coetzee, J. Am. Chem. Soc., 79, (1957) 870.

97. J.F. Coetzee and W.R. Sharpe, J. of Soln. Chem., 1 (1972) 77.

98. P.R. Griffiths, Chemical Infrared Fourier Transform Spectroscopy, John Wiley and Sons, New York, 1975.

99. G. Horlick, Appl. Spectrosc., 22 (1968) 617.

100. J.E. Bertie in J.R. Durig (Ed.), Analytical Applications of FT-IR to Molecular and biological systems, D. Reidel, Boston, 1980, p. 25.

101. A.T. Bell in A.T. Bell and M.L. Hair (Eds.), Vibrational Spectroscopies for Adsorbed Species, American Chemical Society, Washington, D.C., 1980, p. 13.

102. P.R. Griffiths, H.J. Sloane and R.W. Hannah, Appl. Spectros., 31 (1977) 485.

103. J.L. Koenig, Appl. Spectrosc., 29 (1975) 293.

104. J.L. Koenig, Acc. Chem. Res., 14 (1981) 171.

105. P. Venkateswarlu, J. Chem. Phys., 19 (1951) 293.

106. O.A. Pletrii and I.G. Khomichenko, J. Electroanal. Chem., 106 (1980) 277.

107. A.S. Quist, J.B. Bates and G.E. Boyd, J. Chem. phys., 54 (1971) 4898.

108. S.D. Ross, Spectrochim. Acta, 18 (1962) 225.

109. D.E. Irish and M.H. Brooker in R.J. H. Clark and R.E. Hester (Eds.), Advances in Infrared and Raman Spectroscopy, Vol. 2, Heyden, New York, 1976, p. 212.

110. J.C. Evans and G.Y.S. Lo, Spectrochim, Acta, 21 (1965) 1033.

111. J.F. Coetzee and W.R. Sharpe, J. Soln, Chem., 1 (1972) 77.

112. J.P. Devlin and K. Consani, J. Phys. Chem 85 (1981) 2597.

113. S.C. Mohr, W.D. Wilk and G.M. Barrow, J. Am. Chem. Soc., 87 (1965) 3048.

114. M.S. Khatkale and J.P. Devlin, J. Phys. Chem., 83 (1979) 1636.

115. R.E. Hester in R.J. H. Clark and R.E. Hester (Eds.), Advances in Infrared and Raman Spectroscopy, Vol. 4, Heyden, New York, 1978, p. 1.

116. P.C. Li, J.P. Devlin and H.A. Pohl, J. Phys. Chem., 76 (1972) 1026.

117. J. Stanley, D. Smith, B. Latimer and J.P. Devlin, J. Phys. Chem., 70 (1966) 2011.

118. J.C. Moore, D. Smith, Y. Youhne and J.P. Devlin, J. Phys. Chem., 75 (1971) 325.

119. I. Juchnovshi, M.I. Raschkov and I. Panayotov, Monatsh. Chem., 101 (1970) 1712.

120. I.V. Aleksandrov, Y.S. Bobovich, V.G. Maslov and A.N. Sidorov, Opt. Spectrosc., 35 (1973) 154.

121. J.J. Hinkel and J.P. Devlin, J. Chem. Phys., 58 (1973) 4750.

122. C. Takahashi and S. Maeda, Chem. Phys. Lett., 22 (1973) 364.

123. I.V. Aleksandrov. Y.S. Bobovich, V.G. Maslov and A.N. Sidorov, Sov. Phys. JETP Lett., 17 (1973) 219.

124. F.A. Miller, O.Sala, J.P. Devlin, J. Overend, E. Lippert, W. Luder, H. Moser and J. Varchmin, Spectrochim. Acta, 20 (1964) 1233.

125. C. Menard and A. Mellier, Spectrochim. Acta, 29A (1973) 1273.

126. I. Laulicht and S. Pinehas, Israel J. Chem., 1 (1963) 404.

APPENDIX

PROGRAM I

```
FOR XXX = 1 TIL 100
CLS
CLR
OFN = 2
DFN = 21
CAD
OFN = 4
DFN = 20
CAD
FOR III = 1 TIL 30
DSS
NXT III
NXT XXX
END
```

FOR XXX - enables looping sequence

TIL - number of looping cycles

NXT - returns loop to beginning

CLS - collects interferograms and stores in sample file

CLR - collects interferograms and stores in reference file

OFN - origin file number

DFN - destination file number

CAD - adds origin file to destination file with weighting

DSS - display sample file

END - end of program

PROGRAM 2

```
FOR XXX = 1 TIL 50
CLS
CLB
CLR
OFN = 2
DFN = 19
CAD
OFN = 3
DFN = 18
CAD
OFN = 4
DFN = 17
CAD
FOR III = 1 TIL 30
DSS
NXT III
NXT XXX
END
```

CLB - collects interferograms and stores in background file.